2003

The extinction properties of reddened Galactic OB sightlines

Lynne Angela Valencic
Louisiana State University and Agricultural and Mechanical College

THE EXTINCTION PROPERTIES OF REDDENED GALACTIC OB SIGHTLINES

A Dissertation

Submitted to the Graduate Faculty of the
Louisiana State University and
Agricultural and Mechanical College
in partial fulfillment of the
requirements for the degree of
Doctor of Philosophy

in

The Department of Physics and Astronomy

by
Lynne Angela Valencic
B.S., Case Western Reserve University, 1997
December, 2003

Acknowledgments

This work would not have been possible without Geoffrey Clayton for his enthusiastic support, enlightening conversations, endless patience, and excellent advice. He was always there to point out the right direction when I wandered off the trail. Take a bow, Geoff. Take several.

I owe much gratitude to Karl Gordon, who kindly provided me with FM parameters, the software to produce extinction curves, and much encouragement. A very big thank you, Karl. I would also like to acknowledge Michael Wolff for his support and sage advice about database management and things astrophysical.

I have had the pleasure of interacting with and learning a great deal from many people during my time at LSU. I thank Karly Pitman and Tracy Smith for their invaluable friendship, and Christine McGough, Stefan Cartledge, Todd Vaccaro, Mark Slovak, and Kevin Pearson for many enjoyable conversations. Patrick Motl deserves special thanks for his help with IDL and enduring friendship, as does Zed Pobré for his patience and kindness.

I would also like to thank my mentors from older days, Peter Pesch and the late Bruce Stephenson, for their encouragement and friendship. Another child of the Warner & Swasey Observatory heads out into the world.

Last but certainly not least, I would like to acknowledge Kris Valencic and my late parents for their support.

Financial support was provided by the Louisiana Board of Regents, BoRSF, under agreement NASA/LEQSF(1996-2001)-LaSPACE-01 or NASA/LEQSF (2001-2005)-LaSPACE and NASA/LaSPACE under grant NGT5-40115.

Table of Contents

List of Tables

List of Figures

Abstract

A solid understanding of dust grains and their extinction properties is needed to better remove the effects of extinction from data and to comprehend the nature of the processes which modify grains. This requires a large sample of Galactic sightlines, extending far beyond the solar neighborhood, sampling not only a large volume of space but also a wide variety of environments. To fulfill this requirement, a database of sightlines toward 426 young, reddened stars was constructed using extinction curves based on IUE spectra. The curves were fit and the Fitzpatrick-Massa (FM) parameters were found. FM parameters allow for a quantitative analysis of curve characteristics. IR photometry was also obtained for these sightlines, and thus R_V (=A(V)/E(B-V)) was found. Links between the environment and various grain populations responsible for different components of the extinction curve were sought, as were relationships between different FM parameters, especially those which describe the 2175 Å absorption feature (the "bump"). A search for sightlines which cannot be described by the R_V-dependent extinction law of Cardelli, Clayton, & Mathis (1989; hereafter CCM) was also undertaken. The main results are: (1.) The CCM extinction relation is accurate for the vast majority of Galactic sightlines. Thus, processes which lead to a CCM-like extinction curve dominate the ISM and the grain populations responsible for the extinction are modified efficiently and systematically. (2.) The central wavelength of the bump does not shift, and the bump width is environment-dependent, being narrow along diffuse sightlines and broadening with increasing den-

sity. These provide constraints on grain mantle materials. (3.) The Galaxy can support environments that lead to Magellanic Cloud-like extinction; this emphasizes the importance of local environment in determining extinction properties. (4.) Reddened Galactic sightlines which do not adhere to the standard extinction relation tend to be dense and molecule-rich.

1. Introduction

The Earth's atmosphere is very effective at shielding the surface from ultra-violet (UV) photons ($\lambda \cong 3200$ Å- 100 Å). Rayleigh scattering from N_2 and O_2 molecules are primarily responsible, while O_2 and O_3 molecules produce continuum absorption. The combination of these processes essentially prevents all UV photons from hitting the surface (and any ground-based detector.) Thus, UV astronomical observations must be made from either balloon- or rocketborne instruments or, ideally, from space.

The first detections of far-UV (FUV) sources other than the Sun took place in 1955 (Byram et al. 1957), while the first UV stellar spectrophotometry was done by Stecher & Milligan (1962). Three years later, Stecher noted for the first time the existence of what would become famous in UV astronomy as the "bump" at 2175 Å (Stecher 1965.)

The first satellite capable of UV observations, OAO-2, was launched in 1968, and was followed by a host of other satellites (Cox 2000). A listing of major missions is shown in Table 1.1. The data obtained by these instruments are responsible for the vast majority of contributions to observational UV astronomy. This is especially true of studies of the interstellar medium (ISM) and dust, as dust grains preferentially extinguish short-wavelength light. By comparing heavily extinguished stars against their intrinsic fluxes, we can better understand grain properties and composition. This is important for two reasons. First, solid knowledge of grain properties will allow us to build more realistic grain models and correct for the effects of dust in stellar and

galactic photometry and spectra more accurately. Second, dust grains are extremely sensitive to their environment, and can yield much information about local conditions and the physical and chemical processes which affect grains.

A common method used in studies of the ISM is the pair method (Bless & Savage 1970). In their work, Bless & Savage (1970) noted that the flux ratios of several pairs of unreddened stars of the same spectral and luminosity types were extremely similar. They thus concluded that any differences between the UV spectra of stars of the same spectral classification were due to the intervening ISM, and went on to construct extinction curves of sightlines from four different star forming regions, noting that all had the 2175 Å bump and a rapid rise in the FUV, and that these were attributable to the ISM. Many authors since then have used extinction curves to study the ISM in the Milky Way (York et al. 1973; Nandy et al. 1975; Nandy et al. 1976; Koorneef 1978; Seaton 1979; Snow & Seab 1980; Kester 1981; Meyer & Savage 1981; Aiello et al. 1982; Massa et al. 1983; Massa & Savage 1984; Savage et al. 1985; Fitzpatrick & Massa 1986, 1988, 1990, hereafter FM86, FM88, FM90; Clayton & Fitzpatrick 1987; Aiello et al. 1988; Cardelli et al. 1988, 1989, hereafter CCM; Papaj et al. 1991; Papaj & Krelowski 1992, and Jenniskens & Greenberg 1993 to name a handful) as well as in other galaxies (Borgman et al. 1975; Nandy et al. 1981; Koorneef & Code 1981; Clayton & Martin 1985; Fitzpatrick 1985, 1986; Clayton et al. 1996; Bianchi et al. 1996; Gordon & Clayton 1998; Misselt et al. 1999). A sample Galactic extinction curve is shown in Fig. 1.1.

Table 1.1: Major Spaceborne UV Telescopes

Satellite	Years of Operation
OAO-2	1968-1973
Copernicus	1972-1980
TD-1	1978-1996
ANS	1974-1977
IUE	1978-1996
HST	1990-present
EUVE	1992-2001
FUSE	1999-present

A very important technique in the analysis of UV extinction curves is Fitzpatrick-Massa (FM) parameterization (FM86, FM88, FM90). In it, a single function is used to fit a curve. The quantity x is defined to be λ^{-1} and is expressed in units of $\mu\mathrm{m}^{-1}$; in FM90, the function is fit from 3.3 to 8.7 $\mu\mathrm{m}^{-1}$. This is further discussed in Chapter 2. The entire function is given by

$$\frac{E(\lambda - V)}{E(B - V)} = c_1 + c_2 x + c_3 D(x; \gamma, x_0) + c_4 F(x) \tag{1.1}$$

where

$$D(x; \gamma, x_0) = \frac{x^2}{(x^2 - x_0^2)^2 + (x\gamma)^2} \tag{1.2}$$

and

$$F(x) = 0.5392(x - 5.9)^2 + 0.05644(x - 5.9)^3 \tag{1.3}$$

for $x \geq 5.9\mu\mathrm{m}^{-1}$ and $F(x) = 0$ for all other x.

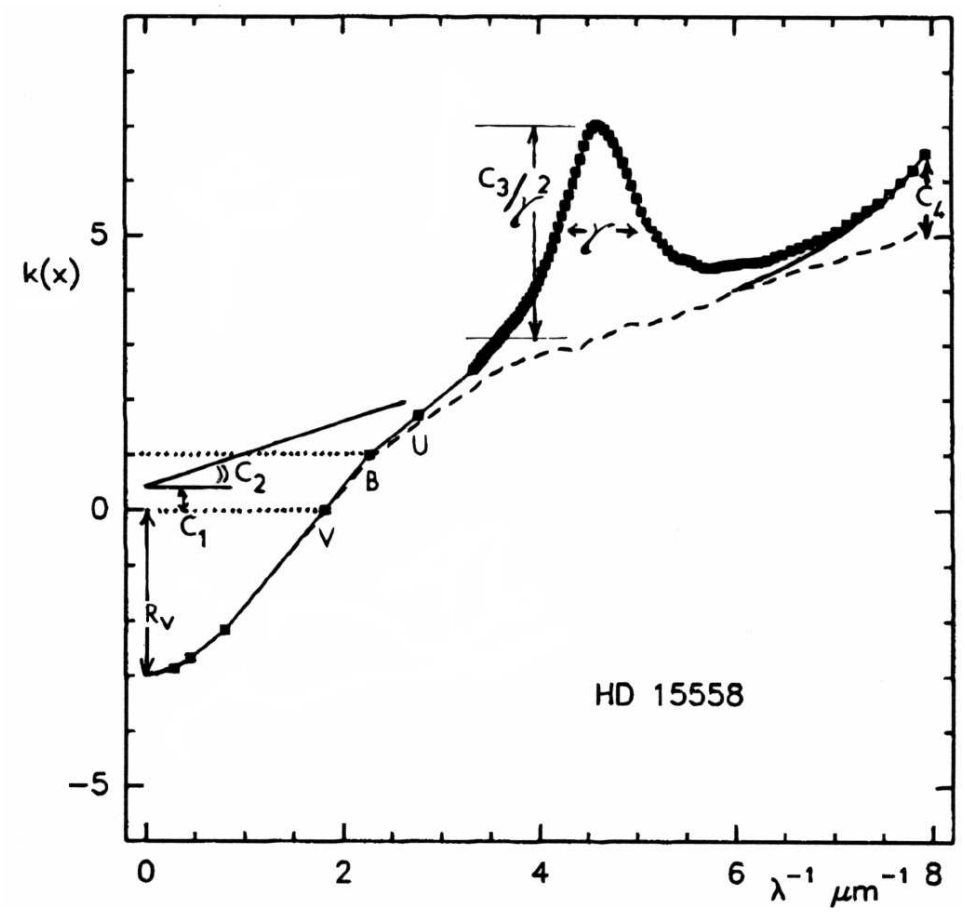

Figure 1.1: Extinction curve of HD 15558, with definitions of the FM parameters. The extinction is plotted in terms of E(λ - V)/E(B-V) against $1/\lambda$ (μm^{-1}). From Jenniskens & Greenberg (1993).

In the first two terms of eq. (1.1), c_1 and c_2 account for the intercept and slope of the linear background. They are not independent of each other and can be merged into one parameter (Carnochan 1986, FM88), though that is not done here. The quantities c_3 and c_4 correspond to the strength of the bump and the curvature of the FUV rise. The last two parameters, x_0 and γ, correspond to the central wavenumber and width of the bump,

respectively; x_0 does not vary greatly from sightline to sightline, so it may be possible to reduce the number of parameters to four overall (Fitzpatrick 1999). The bump is fit by a variation on a Lorentzian profile, often called a Drude profile, which is the expression for the absorption cross section due to a forced damped harmonic oscillator (Jackson 1962, FM90). The bump strength has been defined as both $\frac{c_3}{\gamma^2}$ and $\frac{\pi c_3}{2\gamma}$; the first is the height of the bump with respect to the linear background and the second is the area under the Drude fitting function. The great advantage to this parameterization is that is allows for meaningful comparisons of extinction curve characteristics from sightline to sightline.

A major leap forward in understanding interstellar extinction occured in 1988, when CCM published their findings on a mean extinction relation that depended on one parameter, the ratio of total-to-selective extinction, R_V (=A(V)/E(B-V)). With only very few exceptions, Galactic extinction curves tend to follow this law within the uncertainties of the calculated R_V values and the extinction curves (Clayton et al. 2000, Fitzpatrick 1999). The Galactic diffuse ISM is well described by a curve where $R_V = 3.1$. R_V can also be thought of as a rough indicator of grain size, with low R_V sightlines having more small grains than high R_V sightlines. The CCM extinction relation generally does not apply outside the Galaxy, although recent work has shown that there are sightlines toward the LMC which may follow CCM (Gordon et al. 2003). This law essentially replaced the Galactic average extinction curve (Seaton 1979) with a family of R_V-dependent extinction curves, with each curve representing a mean curve for sightlines of that particular value

of R_V. This also showed that many of the so-called "anomalous" sightlines (e.g. Clayton & Fitzpatrick 1987) were in fact normal. See Fig. 1.2.

In addition to finding this relationship, CCM pointed out the usefulness of normalizing extinction curves to A(V), rather than E(B-V), as was usually done. This renormalization is done by dividing the curves by their measured R_V. Compared to E(B-V), A(V) is a more basic quantity; E(B-V) is the difference between the extinction in the B and V bands. A(V) is also a direct measurement of the optical depth along a sightline. Normalization to A(V) can better show the relationship between FM parameters (CCM; Jenniskens & Greenberg 1993; Fitzpatrick 1999). In doing so, the implicit R_V term in the E(B-V)-normalized curve is divided out and the result can then be compared to R_V in a meaningful way. This renormalized curve $\frac{A(\lambda)}{A(V)}$ can be found through eq. 1.4. FM parameters can easily be normalized to A(V) as well, see eqs. 1.5 and 1.6 (CCM, FM90, Jenniskens & Greenberg 1993). The parameters which describe the bump width and position, γ and x_0, are not affected by the choice of scale (FM90, Jenniskens & Greenberg 1993).

The existence of the R_V-dependent extinction relation implies that the physical processes which alter grains' physical compositions and sizes affect grains of all sizes simultaneously and efficiently, and establishes a general correlation between grain environment and the wavelength dependence of extinction (CCM, Fitzpatrick 1999).

$$\frac{A(\lambda)}{A(V)} = \left(\frac{E(\lambda - V)}{E(B - V)}\right) \frac{1}{R_V} + 1 \tag{1.4}$$

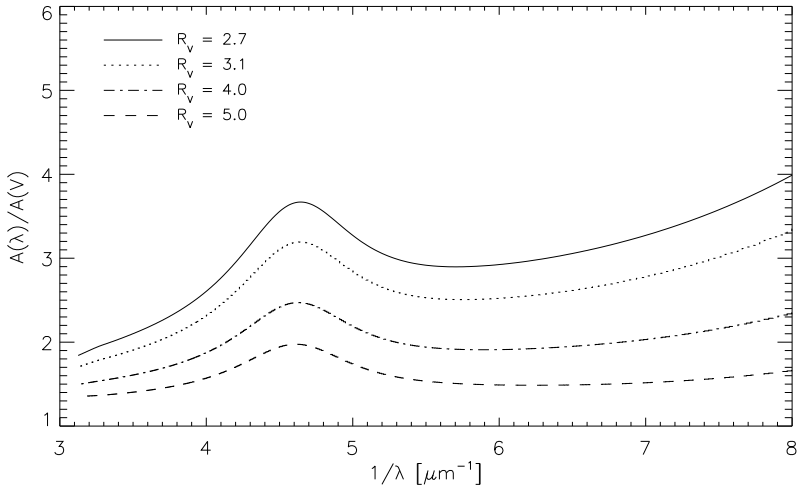

Figure 1.2: CCM extinction curves for $R_V = 2.7$, 3.1, 4.0, and 5.0.

$$c_1^{A(V)} = c_1^{E(B-V)}/R_V + 1 \tag{1.5}$$

$$c_{2,3,4}^{A(V)} = c_{2,3,4}^{E(B-V)}/R_V \tag{1.6}$$

There are significant differences between dust grains and the extinction curves they produce in the Galaxy and those found in the Small and Large Magellanic Clouds. Fig. 1.3 shows the typical Galactic diffuse ISM curve for $R_V = 3.1$ and average curves from the SMC Bar, the LMC Supershell, and the average LMC (Gordon et al. 2003). Longward of about 3 μm^{-1} these curves are about the same, but differences appear toward shorter wavelengths. Of these curves, the SMC Bar is the most extreme, having no bump but very strong FUV extinction that is linear with $1/\lambda$. The two LMC curves

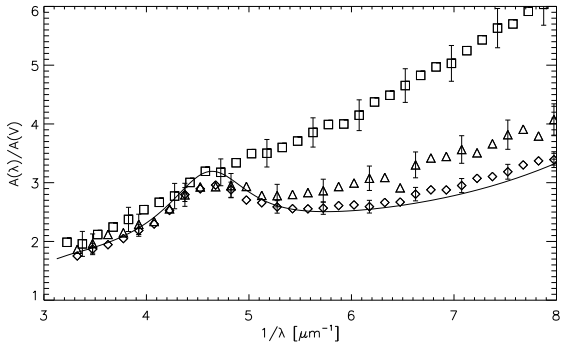

Figure 1.3: Top: Extinction curves of the average LMC (diamonds), LMC2 Supershell (triangles), SMC Bar (squares), and CCM R_V=3.1 (solid line). Magellanic Cloud data is from Gordon et al. (2003).

have weak bumps compared to CCM R_V=3.1, but stronger FUV extinction, though not as strong as the SMC. There are also significant differences in metallicities and the gas-to-dust ratios. The gas-to-dust ratio for the Galaxy is N(HI)/A(V)= 1.55 $\times 10^{21}$ cm^{-2} mag^{-1} (Bohlin et al. 1978), while for the SMC Bar N(HI)/A(V)=13.18 $\times 10^{21}$ cm^{-2} mag^{-1} and the average LMC has N(HI)/A(V)=3.25 $\times 10^{21}$ cm^{-2} mag^{-1} (Gordon et al. 2003). These very different ratios may indicate the level of dust self-shielding that is possible in these areas, in that in regions where self-shielding is high, the dust may not have an environment conducive to forming dense (and protective) clouds. The metallicity of the Clouds is much lower than the Galaxy, with [Fe/H]≈ -0.3 for the average LMC and [Fe/H]≈ -0.6 for the SMC, though there is wide variation (Luck & Lambert 1992).

As Bless & Savage (1970) noted, extinction curves in the Galaxy have two characteristic features: the 2175 Å bump and a rapid rise in the FUV. The exact identities of the feature carriers are not known. The most likely carrier of the bump is believed to be graphite grains (Stecher 1965; Savage 1975; Mathis et al. 1977; Hecht 1981; Cardelli & Savage 1988; Draine 1989; Mathis & Whiffen 1989; Sorrell 1990; Clayton et al. 1992; Draine & Malhorta 1993; Mathis 1994; Will & Aannestad 1999) though other carriers have been considered, including polycyclic aromatic hydrocarbons or PAHs (Lee & Wdowiak 1993, Duley & Seahra 1998, 1999), coal (Papoular et al. 1996), and spherical, multi-shelled fullerenes or carbon onions (Henrard et al. 1993, 1997; Ugarte 1995). The only non-carbonaceous suggestion is OH^- molecules on small silicate grains (Steel & Duley 1987), though this was deemed rather unlikely (Draine 1989; Mathis 1994) as the fraction of Si atoms bonded to OH^- molecules was not consistent with observations. The FUV rise is commonly attributed to silicate grains (Mathis et al. 1977; Hong & Greenberg 1980; Draine & Lee 1984; Weingartner & Draine 2001) although, again, PAHs have been invoked by some (Léger et al. 1989; Jenniskens et al. 1992; Désert et al. 1995; Li & Greenberg 1997).

It is also possible for grains in sheltered areas like dark clouds to grow mantles of organic molecules and/or ices (Hecht 1981; Goebel 1983; Draine 1989; Tielens 1989; Whittet 1992; Mathis 1994; Beegle et al. 1997). Whittet (1992) describes a typical mantled grain as possessing a core of silicates or amorphous carbon with a coating of water or ammonia ice, then a second mantle of molecular oxygen, nitrogen, or carbon monoxide. It has also been

suggested that refractory metals such as Fe or Mg may form mantles on carbonaceous grains (Mathis 1994; Sofia et al. 1994). Mantles tend to broaden the bump; hence, it is believed that unmantled graphite grains cause the narrowest bumps (Hecht 1981; Goebel 1983; Mathis 1994). It is suggestive that narrow bumps are seen in areas of high radiation, as this would remove any mantles from the graphite (Mathis 1994).

Despite all the work with extinction curves that has been done, a coherent database of Milky Way extinction curves does not exist; the curves cannot in all cases be compared to each other. This is because different authors used variations of the pair method; for example, some used model spectra instead of unreddened stellar spectra, while others produced unreddened spectra for classes they did not have by averaging the unreddened spectra of earlier and later classes, and others used only unreddened spectra. Some authors used the MK spectral types of the reddened sightlines to determine the proper comparison spectra, while others used the unreddened spectra that most closely matched the features of the reddened ones. Different authors used data from different instruments. Also, these sightlines are not necessarily representative of the entire Galaxy, as they do not extend far beyond the solar neighborhood, confining us to local environments. Moreover, not all extinction curves have FM fits and thus cannot be compared quantitatively, and those sightlines that are parameterized are typically normalized to E(B-V). As previously discussed, normalization to A(V) is preferable. Until the recent release of 2MASS data, JHK photometry was available for only a fraction of the stars in the sample. Thus, a coherent picture of extinction in

the Galaxy could not be drawn. Without this, not only can we not properly account for extinction in data where dust is not the subject of study (and its effects need to be removed), but we also cannot hope to make meaningful comparisons to dust grains and their environments in other galaxies.

In order to solve this problem, I have built a cohesive database of over four hundred extinction curves constructed in a uniform manner, using unreddend comparison spectra matched to the reddened UV spectral types. All of these sightlines now have IR photometry, and thus values for R_V and A(V). The extinction curves have been normalized to A(V) and their FM parameters have been found, allowing for a quantitative comparison from sightline to sightline. Over one hundred of these sightlines extend beyond three kpc, thus sampling a much larger volume of the Galaxy than ever before. This is a much larger and more complete database than any done previously; the vast majority of extinction curve studies up until now either do not normalize to A(V) (e.g. Savage et al. 1985; Aiello et al. 1988; Papaj et al. 1991; Jenniskens & Greenberg 1993; Morbidelli et al. 2000; Barbaro et al. 2001). or do not consider FM parameters (Papaj et al. 1991).The 426 sightlines used here is more than double any previous study, with the exception of Savage et al. (1985); they had 1415 sightlines, but did not normalize to A(V) or find the UV spectral type, using the MK spectral type instead. Moreover, Savage et al. (1985) used photometry from ANS, rather than IUE spectra. Thus, they were restricted to finding the extinction in ANS' five passbands (with central wavelenths λ = 1550, 1800, 2200, 2500, and 3300 Å). In comparison, IUE spectra cover a range from 1150 - 3300 Å at a resolution of 5 Å. This

is by far the most complete study. Figure 1.4 shows the distribution of previously published sightlines in the Galaxy with FM parameters normalized to E(B-V) and the sightlines in this new database for which we have FM parameters normalized to A(V). Because of our much larger sample, we have more complete coverage of nearby associations and more distant sightlines than previous works, pushing out further into the Galaxy, and sampling a wider variety of environments. Fig. 1.5 shows the location of the sightlines on the sky with color-coded R_V values. As distances were found using spectroscopic parallax, the uncertainties for stars plotted in Fig. 1.4 are large, with an average uncertainty of 50%. In an effort to make Fig. 1.4 less cluttered, instead of plotting stars that were in open clusters, filled squares were used to indicate clusters with members in the database. As will be shown in following chapters, distances to the program stars, considering their uncertainties, were consistent with distance estimates of the clusters. The database is used to associate specific extinction properties with particular environments, and identify and study sightlines of particular interest, especially those which do not conform to the CCM relation. In one case, HD 204827, I have combined UV data with spectra and images in the IR to construct a comprehensive view of the unusual extinction along this sightline.

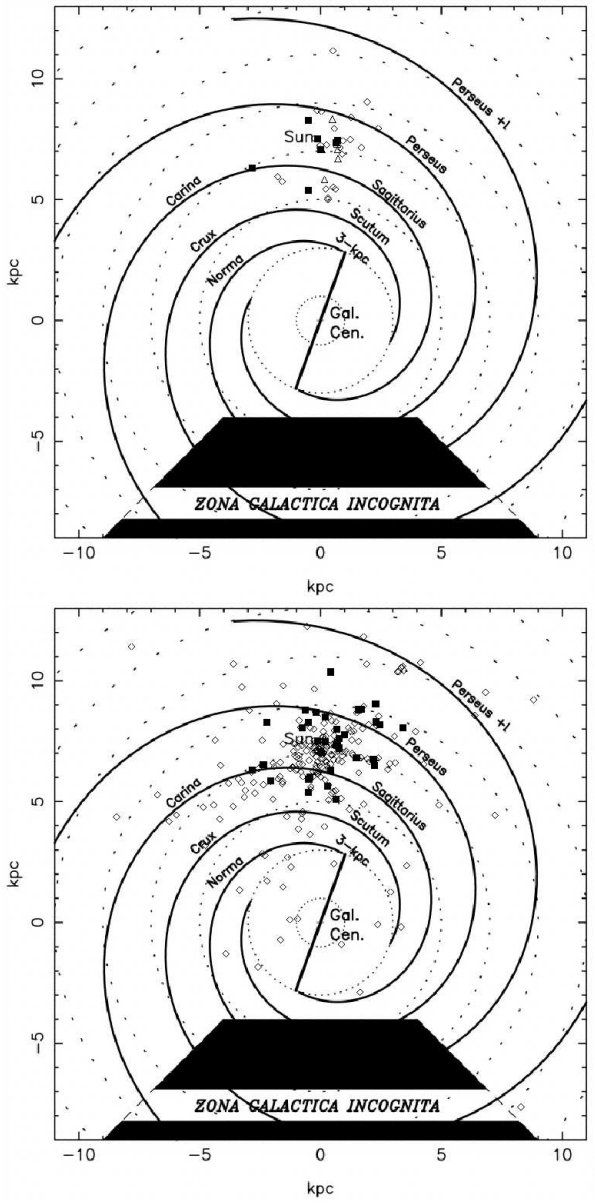

Figure 1.4: Top: Previously published sightlines with FM parameters. Diamonds = FM90; Triangles = Jenniskens & Greenberg 1993; Filled squares = Open clusters with members included in either FM90 or Jenniskens & Greenberg. Bottom: Diamonds = database sightlines for which we have FM parameters normalized to A(V). Filled squares: open clusters with members included in survey. The Galaxy overlay is from Vallée (2002).

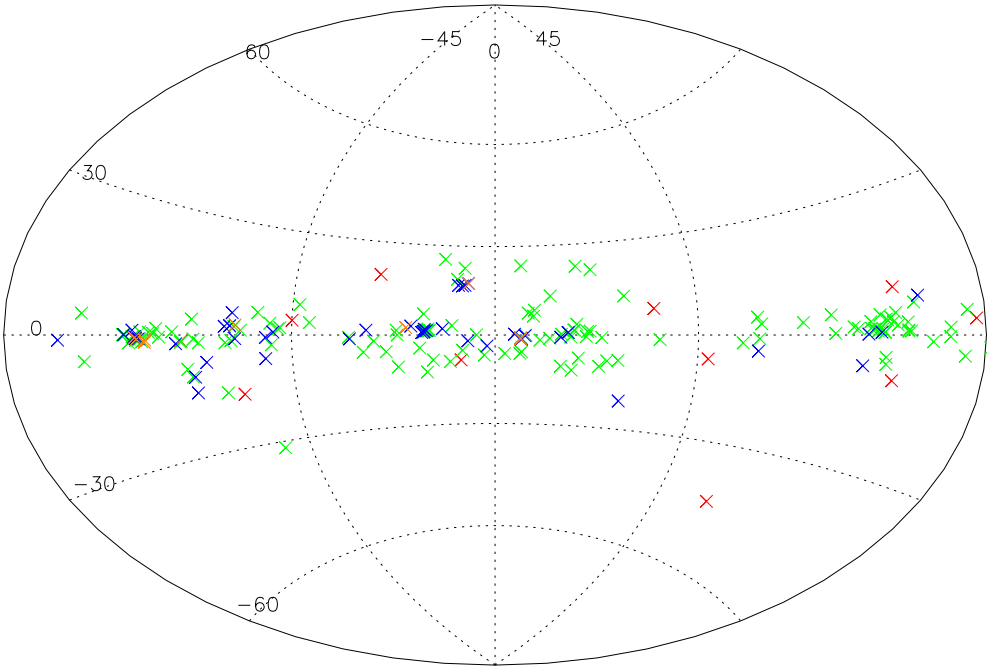

Figure 1.5: Sightlines in the database. Color indicates values of R_V. Red: $R_V < 2.5$, green: $2.5 \leq R_V < 3.5$, blue: $3.5 \leq R_V < 4.5$, yellow: $R_V > 4.5$.

2. Methods

Sightlines observed by IUE between spectral types O3 and B5 were selected for the database, with the exception of HD 29647, a B8 III star, because it is a special case and will be discussed later. This range of spectral types was chosen to minimize the effects of spectral mismatch in their extinction curves; this is discussed further below. (This selection has the added benefit that, being intrinsically bright, they sample a higher volume of space.) Only "normal" stars were included, as without unreddened UV comparison stars that are unavailable for exotic objects, intrinsic spectral energy distributions (SEDs) cannot be completely removed. Any extinction curves made with exotic objects would not accurately reflect the ISM along the sightlines of those objects. Thus, planetary nebulae, novae, mass-transfering binaries, or other such stars were discarded. Stars were bright, with the faintest one in the database being V $\approx$ 11 mag. This is brighter than IUE's limiting magnitude of V $\approx$ 15 mag on low dispersion spectra, which were used to make the curves, because the stars in this study were reddened. Dust preferentially extinguishes light at short wavelengths, so reddened stars fainter than about V = 11 often had little or no flux in the UV and so were removed from the database. The lower limit on E(B-V) was 0.20.

2.1 UV Data

The extinction curves were constructed using low resolution UV spectra from the IUE satellite, specifically the Long Wavelength Primary (LWP), Long Wavelength Redundant (LWR), and Short Wavelength Primary (SWP)

detectors. Often, two apertures were available for a spectrum; the large aperture covered roughly a 10 × 20 arcsec oval and the small one covered a 3 arcsec diameter circle. The spectra were downloaded from the IUE Final Archive; there is a link through the Multimission Archive at Space Telescope Science Institute, http://archive.stsci.edu. As these spectra were from the Final Archive, they were reduced with the standard NEWSIPS processing system and thus generally have higher signal to noise, improved wavelength and flux calibrations, and are more homogeneous than data reduced with the previously used system, IUESIPS (Nichols & Linsky 1996). The long wavelength camera covered $1800 < \lambda < 3300$ Å; the short wavelength camera covered $1150 < \lambda < 2000$ Å. Some sightlines had small aperture spectra as well as large; in these cases, spectra from both apertures were used. This was particularly useful for sightlines that were saturated in the large aperture spectra, but not in the small aperture spectra where the throughput was 60% that of the large aperture. Because the flux calibration for the small aperture was known only relative to the large aperture and not absolutely, small aperture spectra could not be used without corresponding large aperture spectra.

Some sightlines had multiple observations; in these cases, all high S/N spectra were selected and averaged. These reddened spectra were rebinned to the instrumental resolution (5 Å), coadded, and merged. For the sake of homogeneity, Hiltner's photometry (Hiltner 1956, Hiltner et al. 1956) was preferred, when possible, and was obtained for 192 sightlines. In his massive compilation and assessment of UBV photometry, Nicolet (1978) found that

Hiltner's photometry was consistently of high quality. Systematic errors were typically less than 0.01 mag (Hiltner 1956) and photometry agreed well with the works of others (Nicolet 1978). All spectra, photometry, and photometric sources used in this work are listed in an on-line appendix; a link is at http://dirty.as.arizona.edu/ kgordon.

The comparison stars were selected from the IUE Spectral Atlas of Wu et al. (1983) and dereddened assuming $R_V = 3.1$. These stars and their spectral types are listed in Appendix A.

2.2 IR Data

In order to construct R_V dependent CCM curves, IR photometry in the J, H, and K bands was needed. Data for most sightlines were found through IPAC's 2 Micron All Sky Survey (2MASS) archive. Photometry from 2MASS was preferred, but not available for all lines of sight; in these cases, other photometric sources were used.

Values of R_V were found using relations described in Fitzpatrick (1999), see eq. 2.1. These relations were used instead of the often used $R_V = 1.1\frac{E(V-X)}{E(B-V)}$ where X is J, H, or K, because they have been derived from an extinction curve which has been corrected for the changing extinction across the width of the individual filters.

$$R_V = 1.39 \times \frac{E(V-J)}{E(B-V)} - 0.02 \tag{2.1}$$

$$R_V = 1.19 \times \frac{E(V-H)}{E(B-V)} + 0.04 \tag{2.2}$$

Table 2.1: Correlations between values of R_V

$R_V^{The} = (0.77 \pm 0.54) R_V + (1.23 \pm 4.10)$
$R_V^{CCM} = (1.07 \pm 0.12) R_V$ - (0.13 ± 0.40)
$R_V^{Morbidelli} = (0.96 \pm .44) R_V + (0.27 \pm 1.34)$

$$R_V = 1.12 \times \frac{E(V-K)}{E(B-V)} + 0.02 \tag{2.3}$$

Values of R_V were compared to those in the literature; see Fig. 2.1. Our values of R_V tend to agree within the errors with those found earlier. HD 93160, which had an anomalously low R_V, was not included in the fit to Thé et al. (1980); when it was included, the fit did not correlate with our R_V. The overall agreement between our values of R_V and other studies indicates that there is no major bias in our calculated values of R_V and emphasizes that the effect of changing extinction across filters is not very large at the reddenings we are considering, the correction being more of a "tweak" than anything else. Correlations between our values and those in the literature are in Table 2.1.

The average value of R_V was then used to find A(V), as $A(V) = R_V \times E(B-V)$. Spectroscopic parallaxes were then used to find distances. Values of A(V) and R_V are included in the on-line appendix.

2.3 The Pair Method and Extinction Curves

The extinction curves in this work were constructed using the pair method (e.g. FM90), that is, the spectrum for each reddened star was compared to the spectra of unreddened stars until a good spectral match was found. The comparison star was not always of the same MK classification as the program

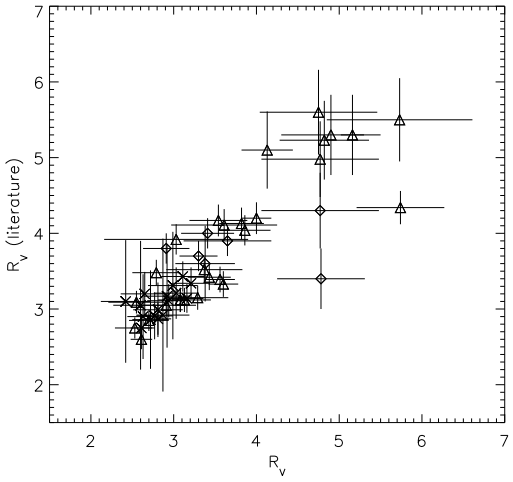

Figure 2.1: Values of R_V taken from the literature versus those derived in this work. X = Morbidelli et al. (1997), diamonds = Thé et al. (1980), triangles = CCM. Error bars indicate 1 σ.

star, since the two stars were matched on the basis of their UV spectra alone. The inherent assumption in the pair method is that the correct comparison spectrum is the one with the same spectral characteristics as the reddened star, and thus the one with the same flux distribution (Cardelli et al. 1992).

Once a reddened spectrum was matched to an unreddened one, the ratio was taken, and the result was converted to magnitudes, so that $\frac{E(\lambda-V)}{E(B-V)} = \frac{m(\lambda-V)-m(\lambda-V)_0}{(B-V)-(B-V)_0}$ (for example, FM90). The curves were then fit and the FM parameters found over the range from 3.7 to 8.0 $\mu\mathrm{m}^{-1}$. The fits are valid only over this modified range (Fitzpatrick 2002, private communication) as opposed to that of FM90, 3.3-8.7 $\mu\mathrm{m}^{-1}$. Thus, the parameters found over the modified range are preferred to those found over the original range. The parameters were found by a three step method. First, the values of x_0 and

Table 2.2: Correlations between FM parameters fit over different ranges

$c_1^{new} = 1.243(\pm.007)c_1^{FM90} + .331(\pm.024)$
$c_2^{new} = 1.022(\pm.009)c_2^{FM90} - .080(\pm.013)$
$c_3^{new} = 0.951(\pm.094)c_3^{FM90} - .208(\pm.032)$
$c_4^{new} = 1.180(\pm.010)c_4^{FM90} - .027(\pm.026)$
$x_0^{new} = 1.023(\pm.173)x_0^{FM90} - .098(\pm.037)$
$\gamma^{new} = 1.073(\pm.023)\gamma^{FM90} - .110(\pm.024)$

γ were held fixed while c_1, c_2, c_3, and c_4 were found by minimizing the χ^2. Second, values for c_1, c_2, c_3, c_4, and γ were held fixed and x_0 was found by minimizing the χ^2. Last, c_1, c_2, c_3, c_4, and x_0 were held fixed and γ was found by minimizing the χ^2. Steps two and three were repeated until χ^2 did not change significantly. This method was preferred over others where the parameters are all found at once because this leads to a smaller χ^2 (Gordon et al. 2003).

In most cases, the parameters found over the original and modified ranges are extremely similar to each other; see Fig. 2.2 and Table 2.2. Four parameters, x_0, γ, c_2, and c_3, are easily within 1 σ of the values found using FM90's range. There is a more substantial difference, however, in c_1 and c_4, as these are both beyond 3 σ of FM90's values; the modified values of c_3 are smaller on average than those found over the classical FM range.

As discussed in Chapter 1, R_V is inherent to the FM parameters. That is, the curves are normalized to E(B-V), so the parameters found by fitting them are also. CCM showed that this is not the most advantageous representation; normalization to A(V) is more straightforward and informative, so the FM parameters found here were converted to "A(V) space" by dividing out R_V

(see Chapter 1 for the equations used). All comparisons and analyses of FM parameters were carried out on these renormalized parameters.

In addition to finding more accurate parameters than in the original FM papers (or any subsequent works), this study includes about 10 times as many sightlines as FM, and about 4 times as many sightlines as studied by Jenniskens & Greenberg (1993), thus increasing the volume of the Galaxy sampled. This is important for establishing trends for Galactic ISM and increases the likelihood of finding unusual environments which may not conform to the CCM relation. Through studying these non-CCM sightlines, a better understanding of the processes which affect grains may be gained.

2.3.1 Distances, Locations, and Cluster Membership

Distances for individual stars were found using spectroscopic parallax, thus the uncertainties are large, sometimes going as high as 50%. The main source of error was the uncertainty in the absolute magntiude for a given spectral type, which was typically on the order of 0.5 mag (Vacca et al. 1996), while the average error in A(V) was $\approx$ 0.1-0.2 mag. The absolute magnitudes were taken from Schmidt-Kaler (1982) and Vacca et al. (1996), and the intrinsic colors were from Schmidt-Kaler (1982) and FitzGerald (1970). Another way to find individual stellar distances, trigonometric parallaxes, also has problems. Hipparcos parallaxes have a random error of about 1 mas (Arenou et al. 1995; Narayanan & Gould 1999), so are not very useful beyond about 500 pc. Parallaxes beyond such distances are subject to large errors and are known to have biases that cannot be corrected for on an individual basis (Smith & Eichhorn 1996; Brown et al. 1997). The majority

(89%) of sightlines in the database extend beyond this distance. Thus, due to the uncertainty in the Hipparcos parallaxes and the wish for homogeneity, the cluster membership was determined by comparing the distance estimates found here and position on the sky to Humphreys' (1978) list of memberships and cluster distances and locations. Humphreys' (1978) distances were found by averaging the distances to cluster members, which were determined by their radial velocity, distance, and location on the sky.

Stars that are known to belong to the same cluster may be thought of as being at roughly the same distance, the average cluster distance. To demonstrate, in Table 2.3, the distances to 18 stars in the open cluster Trumpler 37, derived through spectroscopic parallax, are listed. The generally accepted distance to Tr 37 is about 800 pc (Georgelin & Georgelin 1976), though some have placed it closer; Becker & Fenkart (1971) found it to be around 700 pc away, while Hipparcos parallaxes indicate that it is at 615±35 pc (de Zeeuw et al. 1999). The more distant estimates are in good agreement with the distance found here; see Table 2.3. If the giant (HD 239724), which may not be a cluster member, and HD 205794, which is probably in the foreground, are excluded, the average becomes 757±72 pc. This is still in agreement with previous work, and with few exceptions, is within the uncertainty of the members listed in Table 2.3.

2.3.2 Extinction Curves

There are three major sources of systematic error: spectral mismatches between the program stars and their UV comparison spectra, an undetected companion in the system, and improper dereddening of the comparison spec-

Table 2.3: Trumpler 37 Spectroscopic Parallax Distances

HD	Sp Type	E(B-V)	R_V	Distance (pc)
204827	B0 V	1.10±0.05	2.58±0.12	664^{+284}_{-199}
205794	B5 V	0.62±0.05	3.09±0.26	349^{+162}_{-110}
205948	B2 V	0.50±0.04	2.90±0.27	852^{+356}_{-251}
206267	O6 V	0.52±0.04	2.82±0.22	814^{+328}_{-234}
239683	B5 V	0.54±0.04	2.76±0.22	640^{+258}_{-184}
239689	B5 V	0.45±0.04	2.70±0.29	580^{+238}_{-169}
239693	B5 V	0.41±0.04	2.65±0.29	853^{+344}_{-245}
239710	B3 V	0.62±0.07	3.02±0.32	898^{+480}_{-313}
239722	B5 V	0.93±0.05	2.86±0.17	415^{+188}_{-129}
239724	B1 III	0.62±0.04	3.18±0.24	3064^{+1689}_{-1089}
239725	B5 V	0.52±0.04	3.14±0.28	553^{+240}_{-167}
239729	B0 V	0.66±0.04	3.19±0.19	1120^{+473}_{-333}
239738	B5 V	0.51±0.05	2.90±0.32	459^{+210}_{-144}
239742	B5 V	0.38±0.04	2.36±0.31	877^{+345}_{-248}
239745	B5 V	0.54±0.07	2.66±0.34	545^{+275}_{-183}
239748	B5 V	0.43±0.04	2.93±0.31	547^{+230}_{-162}
BD+57 2395B	B5 V	0.69±0.05	2.44±0.19	1564^{+623}_{-446}
BD+58 2292	B2 V	0.54±0.05	3.00±0.26	724^{+139}_{-116}
			average distance =	862±146 pc

tra (Massa et al 1983). Of these three, spectral mismatch is the largest (Massa et al. 1983; Savage et al. 1985; Aiello et al. 1988). It arises through either temperature or luminosity mismatch. The amount by which the calculated $\frac{E(\lambda-V)}{E(B-V)}$ differs from the correct $\frac{E(\lambda-V)}{E(B-V)}$ depends on $E(B-V)^{-1}$, hence, the more heavily reddened a star is, the smaller the error associated with spectral mismatch (Massa et al. 1983). The equation that describes this is shown in eq. 2.4.

$$\alpha = \left[\frac{\delta m(\lambda - V)_0}{E(\lambda - V)} + 1\right] \times \left[1 - \frac{\delta(B-V)_0}{E(B-V)}\right] \tag{2.4}$$

where α is the ratio of the calculated and true extinctions, that is,

$$\alpha = \left(\frac{E(\lambda - V)}{E(B - V)}\right)_{calculated} / \left(\frac{E(\lambda - V)}{E(B - V)}\right)_{actual} \tag{2.5}$$

and

$$\delta m(\lambda - V)_0 = m(\lambda - V)^{reddened} - m(\lambda - V)^{comparison} \tag{2.6}$$

$$\delta(B - V)_0 = (B - V)_0^{reddened} - (B - V)_0^{comparison} \tag{2.7}$$

As can be seen in eq. 2.4, the error also depends on the difference in the intrinsic (B-V) colors of the comparison and reddened stars. For main sequence O stars, which have very similar intrinsic colors, this is typically a small number ($\leq$0.03) and does not contribute significantly to the overall spectral mismatch error (Massa et al. 1983). However, the intrinsic colors change more rapidly with later spectral types; for instance, the difference in (B-V) between an O5 V and B0 V is 0.03, while for a B0 V and B5 V it is 0.13. Thus, mismatch errors are more likely to affect later spectral types more strongly than earlier ones. For an example of spectral class mismatch, see the top figure in Fig. 2.4. Here, the extinction curve for HD 197512 was derived using a comparison star of the correct spectral type (red curve) and comparison stars that are earlier or later by half a subclass (magenta and violet curves, respectively.) Both mismatched curves are within one σ of the correctly matched one.

There are two main sources of luminosity mismatch error: the intrinsic colors and the strength of the Fe lines (Massa et al. 1983). For O and early B types, the intrinsic colors of giants and dwarfs are very similar; however,

as later spectral types are considered, there is a greater difference in intrinsic colors between stars of the same spectral type but different luminosity class, especially if very luminous classes are considered. For example, from FitzGerald (1970), the intrinsic (B-V) colors of an O9.5 with luminosity class V, III, and Ib are -0.30, -0.30, and -0.27, respectively. In constrast, the intrinsic (B-V) colors of a B5 with luminosity class V, III, and Ib are -0.16, -0.16, and -0.09. Thus, the luminosity mismatch uncertainty in the extinction curves of O and early B stars is not very pronounced. According to Aiello et al. (1988), for early B-type stars, the error associated with one subclass temperature mismatch is comparable to the difference in UV fluxes between a dwarf and giant. The relative smallness of the uncertainty is noteworthy, since for early B stars, luminosity misclassifications are common in the literature (Aiello et al. 1988). The bottom figure of Fig. 2.4 shows extinction curves of HD 197512, where the red curve again is the correct one, and the magenta and violet curves being constructed with comparison stars of the same temperature class but different luminosity classes. Because the effects of spectral mismatching become greater with stars of later spectral type, this study is limited to O3 to B5. There is one exception: HD 29647 (B8 III) in the Taurus Dark Cloud, which has long been known to have an anomalous extinction curve (Cardelli & Savage 1988) and may have grains with water ice mantles (Goebel 1983, Smith et al. 1993).

The Fe lines at 1900 Å also are a potential source of problems. If the lines in the comparison and program stars are not of similar strength, the

resulting extinction curve can have an erroneously shifted bump and a too steep FUV rise (Massa et al. 1983).

In order to gauge the consistency of UV spectral comparisons, I compared the program stars' UV spectral types to those listed elsewhere (Clayton & Fitzpatrick 1988 (CF88), Aiello et al. 1988, Papaj & Krelowski 1992 (PK92)); see Appendix B. These are the same in most cases. Any differences between spectral typing tend to be minimal and are not expected to strongly impact the extinction curves for the reasons given above.

It can be easily seen that an unidentified companion in the system will have only a small effect on the extinction curve if the primary is B5V or earlier and the companion is of a later spectral type (Massa et al. 1983), as both the UV flux and (B-V) color of the system will be dominated by the OB star. However, the IR colors will be influenced by the companion, thus affecting the derived R_V and A(V) values and the distance to the system. If the companion is a more luminous star or a star of comparable spectral type to the primary, the uncertainty increases as there may be more of a contribution to both the UV and visual colors.

Finally, there is the potential for introducing error into the lightly reddened comparison spectra by dereddening them. The comparison spectra were dereddened to the intrinsic UBV colors of FitzGerald (1970) and the JHK colors of Koornneef (1983) and Whittet & Van Breda (1980) using the CCM relation for $R_V = 3.1$. There are two sources of potential error here: dereddening them either too much or too little, and how much the sightline's intervening ISM deviates from CCM. The majority of comparison sightlines

are only slightly reddened, with E(B-V)< 0.10; many were within 1 σ of E(B-V) = 0.

2.3.3 Dense and Diffuse Sightlines

The sightlines were divided into two groups according to the density of material along them. The traditional gauge of this is the reddening per unit distance, E(B-V)/d, or extinction per unit distance, A(V)/d. The drawback to using this is that at large distances, it may fail to show a dense cloud that is significantly impacting the extinction curve (Jenniskens & Greenberg 1993, hereafter JG93). Thus, while a high value of E(B-V)/d or A(V)/d always indicates a dense sightline, a low value can mean either that a sightline truly passes through only diffuse ISM, or that it is simply so long that the higher A(V) from any dense cloud it passes through gets "washed out". Nonetheless, it may still be useful in picking out general trends. JG93 found that sightlines with E(B-V)/d >0.29 mag/kpc tended to cross dense clouds, while those with lower E(B-V)/d usually crossed regions of far lower particle densities. Thus, they designated sightlines with E(B-V)/d < 0.29 mag/kpc 'diffuse', while those with higher E(B-V)/d were considered 'dense'. These criteria, translated to A(V)/d through R_V=3.1, were adopted in this work.

The standard IDL routine CORRELATE was used to find the correlation coefficients to determine if there was a correlation between various parameters. The coefficient of correlation, r, is found by equation 2.8

$$r = \frac{\sigma_{xy}}{\sigma_x \sigma_y} \tag{2.8}$$

where σ_{xy} is the covariance of x and y, and σ_x and σ_y are the standard deviations of x and y. The resulting values of r range from -1 to +1, where -1 indicates a strong negative linear relationship and +1 indicates a strong positive linear relationship. A value of $r \approx 0$ indicates no linear correlation.

Diffuse and dense sightlines, as well as both groups together, with $r >$ 0.20 were fit using the IDL routine LADFIT, which uses the least absolute deviation method to find the best fit line. This was selected over a routine which used χ^2 minimization because it was not strongly influenced by outliers and thus yielded fits that were truer to the data. To illustrate, the FM parameters c_3/R_V and γ are shown in Fig. 2.5. The dashed line shows the best fit line found by minimizing χ^2, while the solid line shows the line found with the least absolute deviation method. The solid line is a better fit to the data. It might be noted, however, that the χ^2 minimization technique yielded best-fit lines that were, within uncertainty, identical to those yielded by the least absolute deviation method in cases where the parameters were tightly correlated. For example, in fitting the relationship between c_1 and c_2, the χ^2 minimization method found that $c_1 = (-3.39 \pm 0.06)\ c_2 + (2.64 \pm 0.04)$. For comparison, the least absolute deviation method found that $c_1 = -3.40\ c_2 + 2.68$.

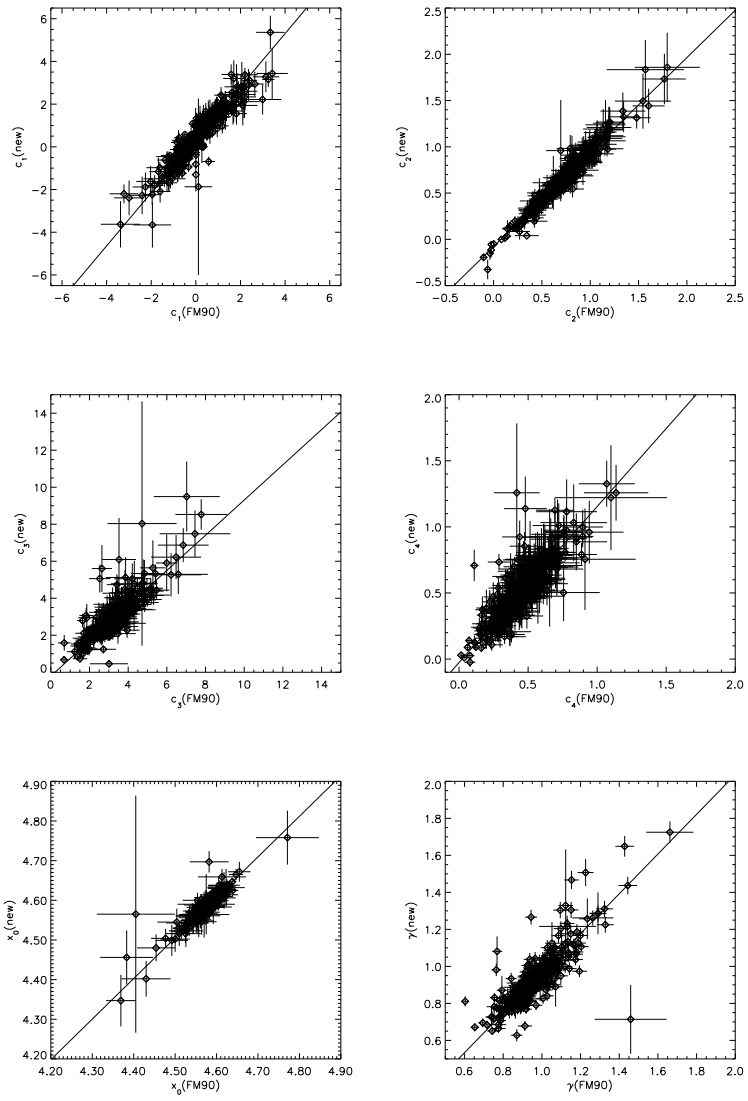

Figure 2.2: Comparison of the FM90 and "new" parameters.

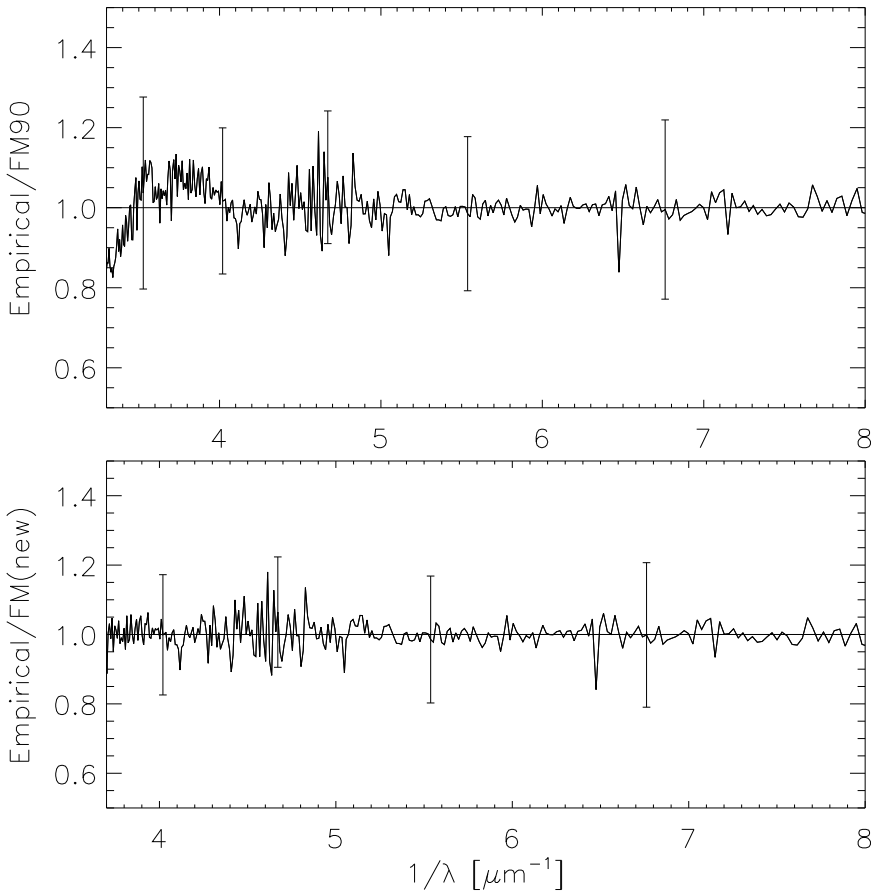

Figure 2.3: The ratio of the empirical IUE extinction curve to the curves made with FM parameters. The top plot uses FM parameters found with FM90's range, while the bottom plot uses a shorter range. Both are plotted over the range of their respective fits.

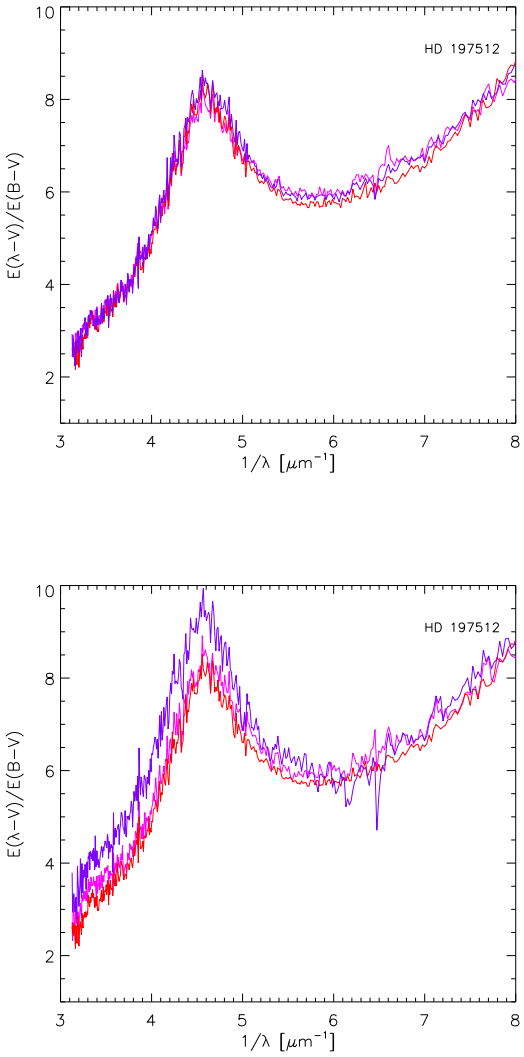

Figure 2.4: Sample mismatches in HD 197512, a B1V with E(B-V)= .35. Top: Mismatches of half a subclass in the spectral type. Red = B1V, magenta = B0.5V, violet=B1.5V. Bottom: Mismatches in luminosity type. Red = B1V, magenta = B1III, violet = B1Ib.

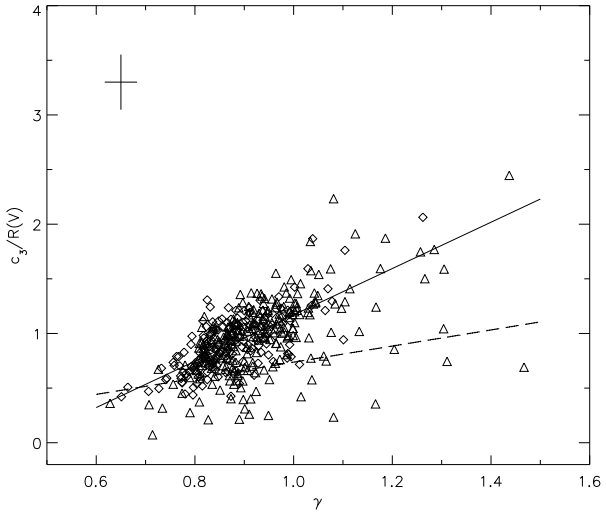

Figure 2.5: FM parameters c_3/R_V vs. γ. Diamond=diffuse, triangle=dense. The dashed line is the best fit found by minimizing χ^2, while the solid line was found by minimizing the absolute deviation.

3. General Trends and CCM/Non-CCM Sightlines in the Galaxy

3.1 General Trends

The parameterization of the extinction curve, first suggested by Savage (1975) and revised through succeeding years by various authors (Seaton 1979; Massa & Fitzpatrick 1986; FM90) is extremely important in that it allows for quantitative comparisons of sightlines. The method by which the parameters were found was discussed in Chapter 2. In order to gain a better idea of the nature of the extinction curves as a whole and the grains responsible for them, the parameters and relationships between them were examined. Similar work was conducted by FM86 and FM88 using a much smaller sample. Plots of FM parameters are shown in the following sections. Representative error bars are shown in all, and the uncertainties for some data points are also shown to give the reader a clearer picture of the errors. Correlation coefficients and best fit line parameters are listed in Table 3.1.

3.1.1 Continuum Extinction

In the top panel of Fig. 3.1, it can be seen that there is a clear correlation between c_1/R_V and c_2/R_V (see Table 3.1). This has been noted before (Carnochan 1986; FM86; JG93). According to FM88, c_1 = -3.00 c_2 + 2.04, while JG93 find that $c_1 = (-3.11 \pm 0.11)\ c_2 + (2.14 \pm 0.07)$. This relation, aris-

ing from the normalization, shows how tightly constrained the background is with respect to A(λ)/A(V) (FM88).

There appears to be a tendency for c_2/R_V to be smaller at higher densities; see Fig. 3.2. Both dense and diffuse sightlines cover approximately the same range, c_2/R_V covering ≈ 0.3. However, higher density sightlines tend to range from $c_2/R_V \approx 0.0-0.3$, while diffuse sightlines appear to be "shifted up" with respect to c_2/R_V and are more likely to have higher slopes, with $c_2/R_V \approx 0.1$ - 0.4. This general environmental dependence was suggested by FM88 and is confirmed here, though FM88 found that their slopes for dense sightlines had a wider range (covering $c_2/R_V \approx$ 0.0-0.4) than that found here ($c_2/R_V \approx$0.0-0.3).

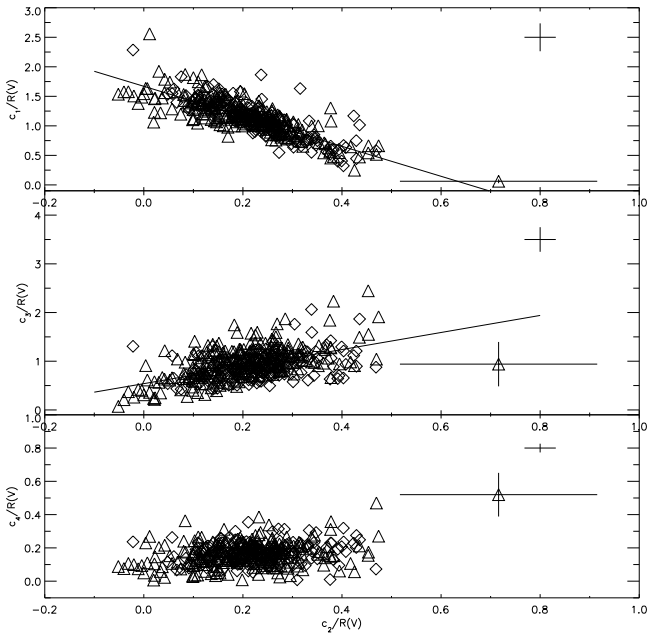

Figure 3.1: FM parameters divided by R_V vs. c_2/R_V. Diamond=diffuse, triangle=dense. A representative 1 σ error bar is shown.

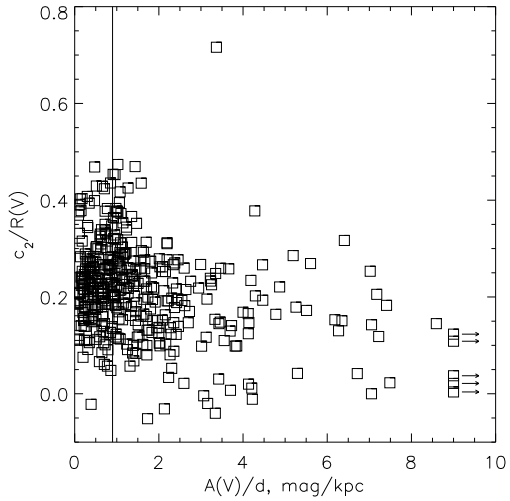

Figure 3.2: FM parameter c_2/R_V and density. The line at A(V)/d=0.9 indicates the cutoff between dense and diffuse sightlines.

The middle panel of Fig. 3.1 shows a weak correlation between c_2/R_V and c_3/R_V. Neither JG93 nor FM86 or FM88 found any apparent relationships between these two parameters. Similarly, in Fig. 3.3, a correlation can be seen between c_2/R_V and the area beneath the bump, $\pi\ c_3/2\gamma$, and the bump height with respect to the background, c_3/γ^2. Both c_2/R_V and c_3/R_V increase with R_V^{-1}, see Fig. 3.4, so perhaps it is not surprising that they themselves are correlated with each other. This may indicate a similarity in the carriers of the background extinction and the bump, or it may reflect a similar environment dependence. As discussed in Chapter 1, it is widely believed that the bump carrier is graphite. It has been suggested that the carrier of the background is primarily amorphous carbon with $a < 0.02\ \mu$m (Jenniskens 1994), but others attribute it to contributions from both silicates

Table 3.1: Correlations between FM Parameters

r	Absolute Deviation	Linear Fit
0.58	0.19	$c_3 = 2.12\ \gamma$ - 0.95
-0.79	0.13	$c_1 =$ -2.54 c_2 + 1.67
0.49	0.54	$c_3 = 1.75\ c_2 + 0.54$
0.49	0.06	$c_2 = 0.11\ \frac{\pi c_3}{2\gamma} + 0.04$
0.31	0.05	$c_4 = 0.05\ \frac{\pi c_3}{2\gamma} + 0.07$
0.41	0.07	$c_2 = 0.13\ \frac{c_3}{\gamma^2} + 0.07$
0.28	0.05	$c_4 = 0.08\ \frac{c_3}{\gamma^2} + 0.07$

and amorphous carbon grains (Clayton et al. 2003), with carbon contributing more extinction toward long wavelengths and silicates affecting UV extinction more strongly than carbon. These populations (amorphous carbon and silicates) are distinct from the bump carrier. Thus, the relationship between these two parameters likely points to environmental dependence.

The bottom panel of Fig. 3.1 shows that c_4/R_V and c_2/R_V are not correlated with each other. This agrees with the findings of FM88 and JG93 and supports the idea that different dust populations contribute to these extinction properties. This is further supported by Fig. 3.5, which shows that c_4/R_V has far less environmental dependence than c_2/R_V. In Fig. 3.5, the diffuse and dense sightlines appear to cover roughly the same range, with $c_4/R_V \approx 0.0$ - 0.4. This is in contrast to c_2/R_V, (see Fig. 3.2), where, as previously discussed, there seems to be a difference in the ranges covered by c_2/R_V which is dependent on environment. If these two populations of grains were affected in a similar way by the local environment, it would be expected that there would be a correlation with the enviroment.

The bottom panel of Fig. 3.6 shows the complete lack of correlation (r=0.13) between c_4/R_V and γ. This is in disagreement with the findings of Carnochan (1986), FM88 and JG93, the latter of whom found a correlation coefficient r= 0.39 for these parameters. It reinforces the idea that factors influencing the bump width are distinct from those influencing the carrier of the FUV rise (FM88).

3.1.2 The 2175 Å Feature: Bump Width

The width of the bump shows real variation and environmental dependence. Values for γ ranged from 0.63±0.03 (HD 24263) to 1.47±0.05. This is a wider range than that reported by FM86, which had values from 0.77±0.09 to 1.25±0.07 μm^{-1}, but this is a much larger sample and covers a larger volume of the galaxy and wider range of environments. The average is 0.92±0.12. HD 29647 and HD 62542 have the broadest bumps in the sample, with $\gamma = 1.467 \pm 0.049$ and $\gamma = 1.304 \pm 0.04$, respectively. The dense and diffuse sightlines have different averages, with dense ones being slightly higher ($\gamma^{avg}_{dense} = 0.95 \pm 0.04$) than diffuse ($\gamma^{avg}_{diffuse} = 0.87 \pm 0.03$). These values are not significantly different from each other, but this likely reflects the density parameter's inability to sort out high versus low densities over long distances, as discussed previously. Next, a z-test was done on the diffuse and dense γ sets. A z-test is a statistical test which can determine if two populations have two different means; it is essentially a t-test for samples with more than 30 data points. The result of a z-test ranges from 0 (the two populations are likely to have two separate means) to 1 (the two populations are likely to have the same mean.) For the dense and diffuse sightlines, the

resulting significance was $\cong 10^{-6}$, which indicates that γ is environmentally dependent. In the top panel of Fig. 3.7, the bump width is plotted against the density A(V)/d for all sightlines in the database. In the top right panel, only the most diffuse sightlines (and thus the most distant, with d > 2 kpc) are shown. Finally, in the bottom panel of Fig. 3.7, only those values of γ beyond 3σ of the mean are plotted. In all, the line at A(V)/d=0.9 indicates the cutoff between dense and diffuse sightlines. The average γ for the low density group in the bottom plot of Fig. 3.7 is 0.80±0.04, while the average for the high density group is 1.12±0.11. This is almost, but not quite, 3 σ. The large uncertainty can be attributed to the increased scatter in the dense groups as opposed to the diffuse group. It can be seen that there is a clear trend that the narrowest bumps tend to be found along sightlines with A(V)/d<0.9.

In Fig. 3.6, the parameters c_2/R_V, c_3/R_V, and c_4/R_V are plotted against γ. The top plot shows that there is essentially no relationship between c_2/R_V and γ, in agreement with FM88 and JG93. This is an interesting contrast to the correlation found earlier between c_2/R_V and c_3/R_V and those two parameters' dependence on R_V. As can be seen in Fig. 3.4, there is a weak correlation between γ and R_V. This supports the assertion that γ is dependent on the environment, as R_V is a general indicator of grain size, which reflects environmental conditions.

The middle panel of Fig. 3.6 shows the well-known relationship between γ and c_3/R_V. Values of c_3/R_V are more confined at lower γ, but as γ increases, c_3/R_V widens its range, with a general trend to increase with γ. This

was noted by both FM88 and JG93, and has been attributed to the fitting procedure (JG93) but FM88 suggested that these two parameters are truly related in some way.

To further demonstrate the bump width's environment dependence, γ, c_3/R_V, and c_4/R_V were compared. In Fig. 3.8, the bump height (c_3/R_V) and FUV curvature (c_4/R_V) are plotted with respect to bump width. The top figure shows all sightlines. Values of γ were split into three categories, each roughly pertaining to environment, with diamonds indicating $\gamma < 0.9$, triangles for $0.9 < \gamma < 1.1$, and squares for $\gamma > 1.1$. To make any correlations easier to see, sightlines in the three different γ categories were plotted separately. The second plot shows the sightlines with the lowest γ, while the third shows those with the middle values of γ and the last shows those with the highest. Narrow bumps ($\gamma < 0.9$) tend to have low bump heights ($c_3/R_V < 1.3$) and can have steep FUV extinction ($c_4/R_V < 0.35$); wider bumps ($0.9 < \gamma < 1.1$) tend to have higher values of c_3/R_V ($c_3/R_V < 1.6$), with only three sightlines having higher values in this γ range) but similar FUV extinction; and broad bumps ($\gamma > 1.1$) have a wide range of c_3/R_V and low FUV extinction.

These results expand upon those of FM86 and Cardelli & Clayton (1991), who found that lines of sight that passed through bright nebulosities had narrower bumps than those that passed through dark clouds, as the "diffuse" and "bright nebulosity" categories are similar.

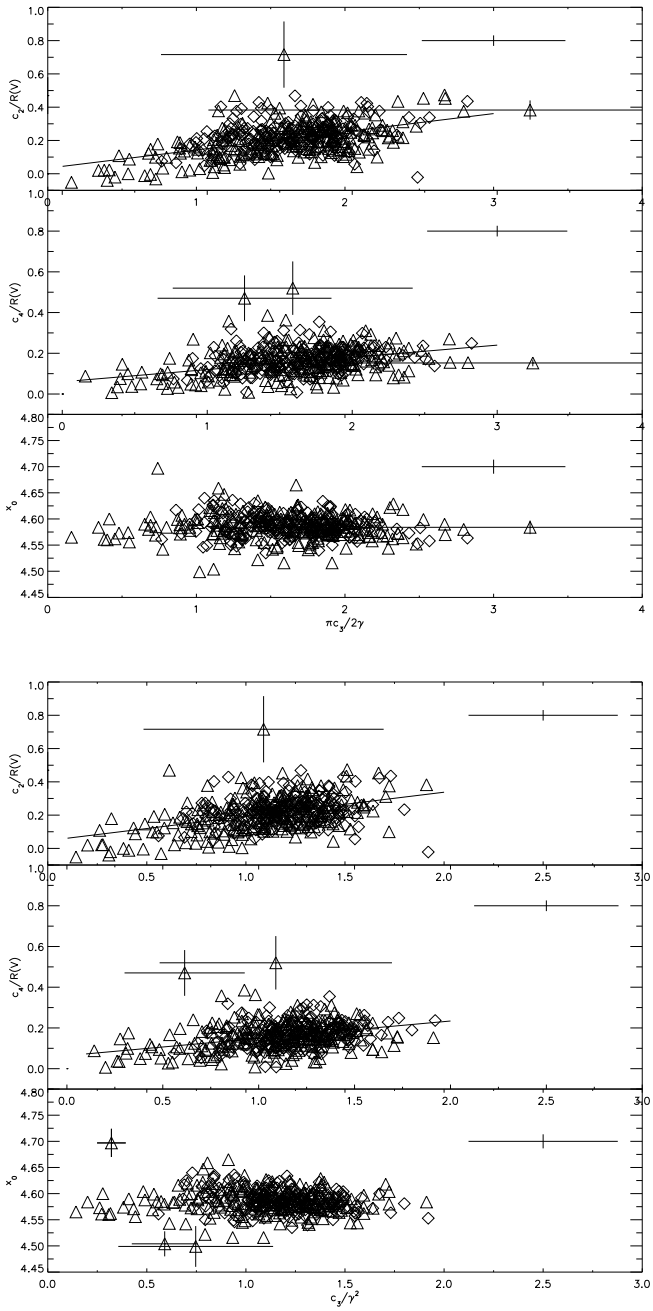

Figure 3.3: FM parameters divided by R_V plotted against the area beneath the fitted bump ($\pi c_3/2\gamma$) and the bump height with respect to the linear background (c_3/γ^2). Diamond=diffuse, triangle=dense. A representative 1 σ error bar is shown.

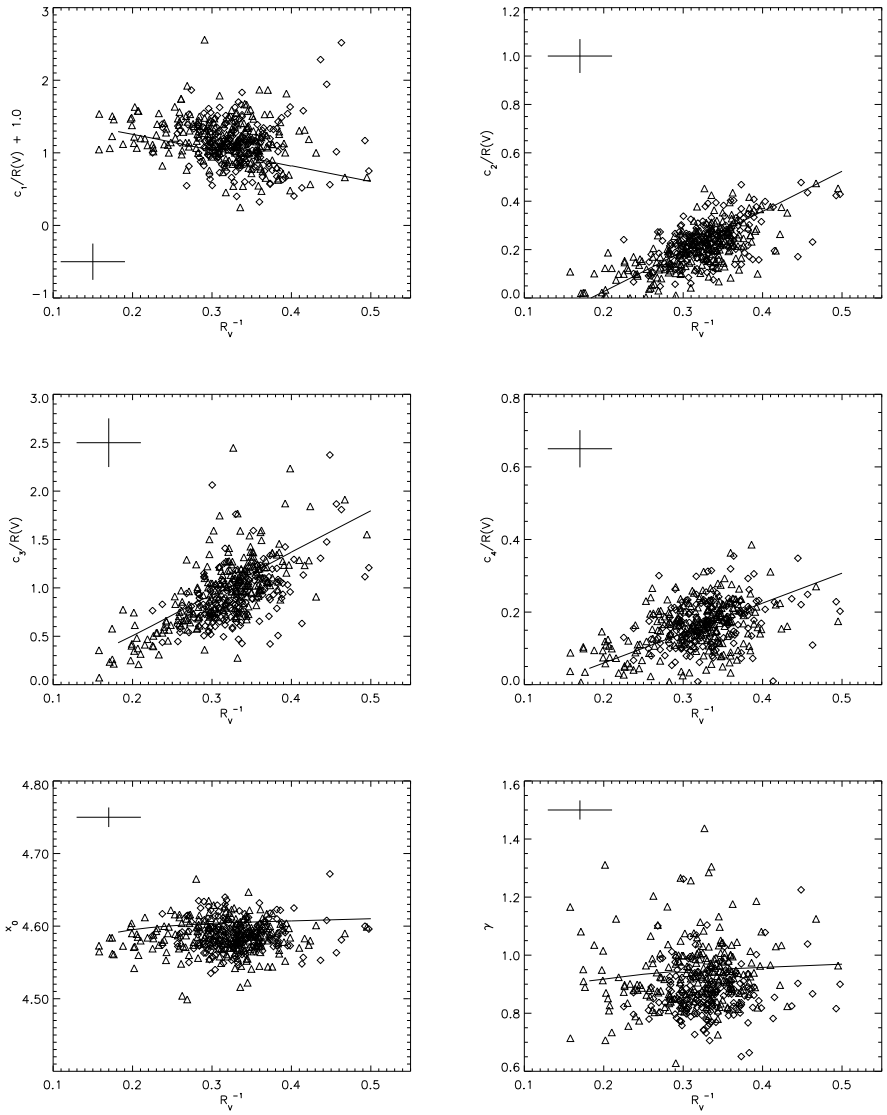

Figure 3.4: The FM parameters for CCM-like extinction curves are plotted with the symbol denoting density; triangles: dense, diamonds: diffuse. The solid line is the CCM relation. Representative error of bars of 1 σ are shown.

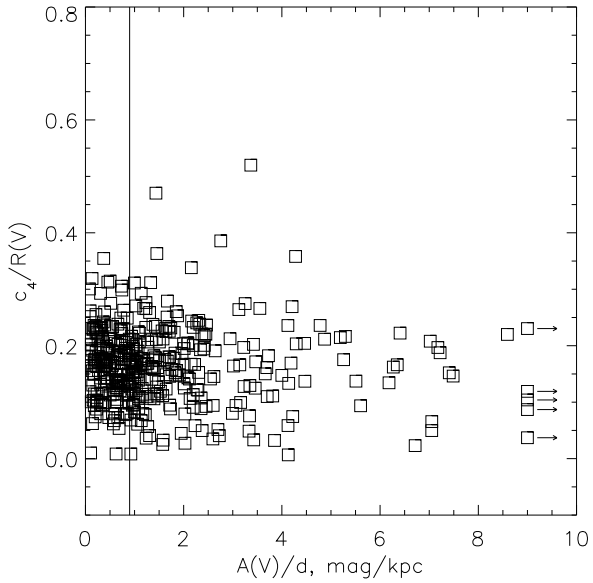

Figure 3.5: FM parameter c_4/R_V and density. The line at A(V)/d=0.9 indicates the cutoff between dense and diffuse sightlines.

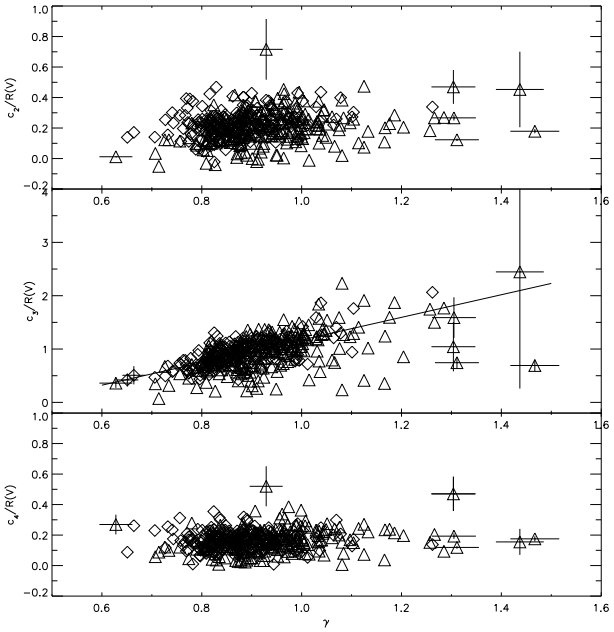

Figure 3.6: FM parameters divided by R_V vs. γ. Diamond=diffuse, triangle=dense.

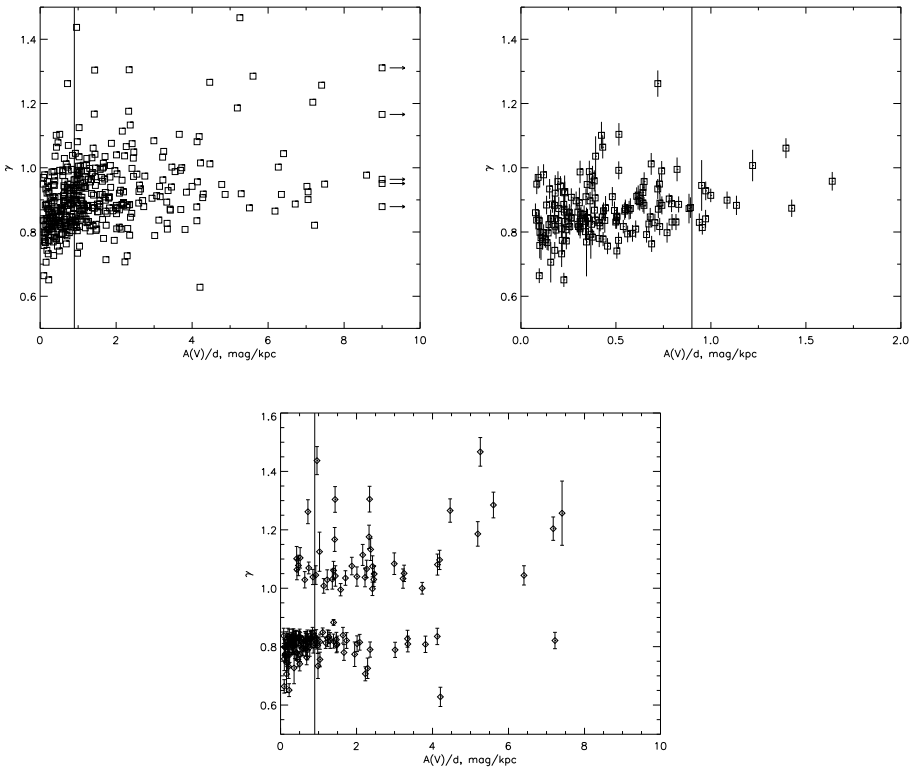

Figure 3.7: Bump width plotted against density. Top panel: entire database; middle panel: sightlines for which d $>$ 2 kpc; bottom panel: γ values beyond 3σ of the mean. The line at A(V)/d=0.9 indicates the cutoff between dense and diffuse sightlines.

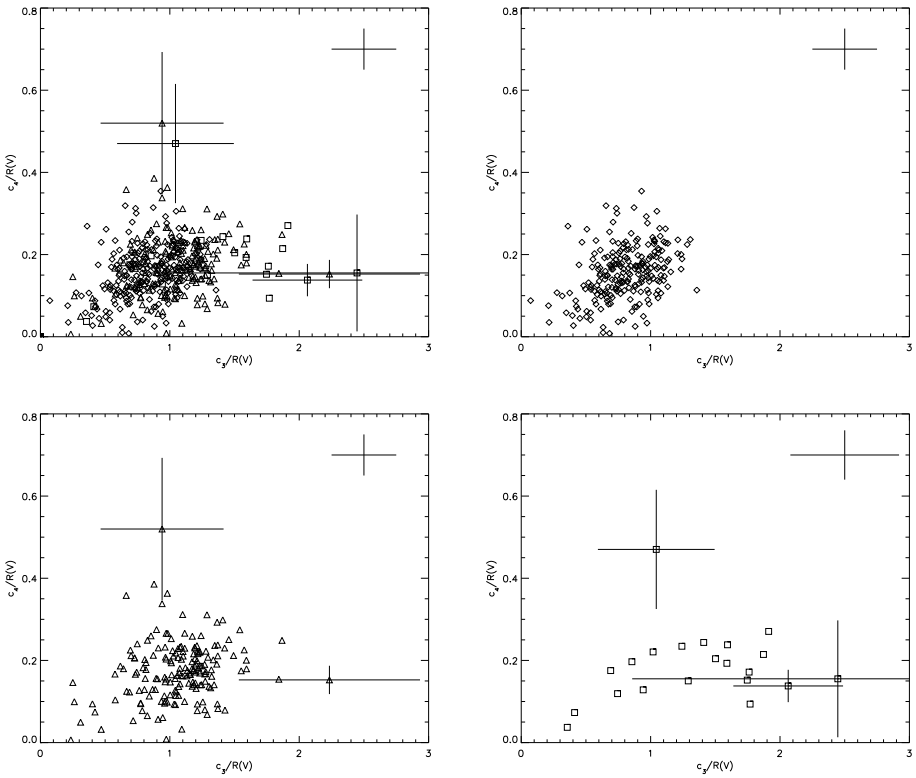

Figure 3.8: c_4/R_V vs. c_3/R_V. Symbols denote values for γ. Diamond: $\gamma < 0.9$, triangle: $0.9 < \gamma < 1.1$, square: $\gamma > 1.1$. A representative 1 σ error bar is shown.

3.1.3 The 2175 Å Feature: The Central Wavelength

There are no correlations between x_0 and any other parameter. In Fig. 3.9, the total lack of correlation between the central position of the bump, x_0, and the bump width, γ, can be seen. The correlation coefficients for x_0 and the other parameters are in Table 3.2. In Fig. 3.9, it can be seen that only one sightline, HD 29647, is significantly shifted, though that is just barely 3 σ from the mean. It is also has a very broad bump, with $\gamma = 1.467 \pm 0.049$. This is interesting because it is thought that grain mantles may cause the bump to both shift and broaden. This sightline will be discussed in detail later. The lack of correlation and extremely narrow range of x_0 values agree with FM86's work, who found that the mean $<x_0> = 4.60$, with their extreme values being within 0.04 μm^{-1} of this. Neither HD 62542 nor HD 29647 were included in FM86's sample. JG93 found a similar value of $<x_0> = 4.58 \pm 0.01$ for Aiello et al.'s (1988) sample. For the sample studied here, $<x_0> = 4.59 \pm 0.01$, with values ranging from 4.50±0.04 (HD 145792) to 4.70±0.03 (HD 29647).

Several authors have tried to link shifts in x_0 to environment. JG93 claimed that bumps in HII regions were shifted to longer wavelengths and broadened. The sightlines that JG93 claimed were shifted all have database values of x_0 that were within 3σ of the mean. Nevertheless, to see if a trend was discernable, the x_0 and γ of JG93's HII set were compared to those of the same stars found here. The result is in Fig. 3.10. The stars are from JG93's list of FM parameters. JG93 state that the average uncertainty in their sample is comparable to that in Massa & Fitzpatrick (1986), so that $\sigma(x_0)$ and $\sigma(\gamma)$ are ≈ 0.01 and ≈ 0.04, respectively. These uncertainties are

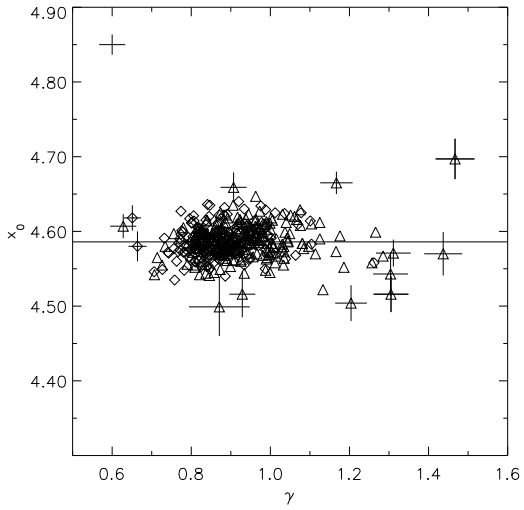

Figure 3.9: FM parameters x_0 vs. γ. Diamond=diffuse, triangle=dense. A representative 1 σ error bar is shown.

Table 3.2: Correlations Between x_0 and Other Parameters

	$c_1/R_V + 1.0$	c_2/R_V	c_3/R_V	c_4/R_V	γ
x_0	-0.08	0.06	-0.05	0.04	0.08

shown, as the uncertainties for the individual parameters are not provided. The squares are the database values for the same sightlines; the correlation coefficient is r=-0.04. Clearly, there is no relationship between these parameters. Thus, with the possible exception of HD 29647, it appears that x_0 is not environment dependent (or at least, if it is, its shifts are within the uncertainties of the measurements) and may in fact be regarded as constant.

Cardelli & Savage (1988) found that both HD 62542's and HD 29647's bumps were significantly shifted to shorter wavelengths. Only one of these

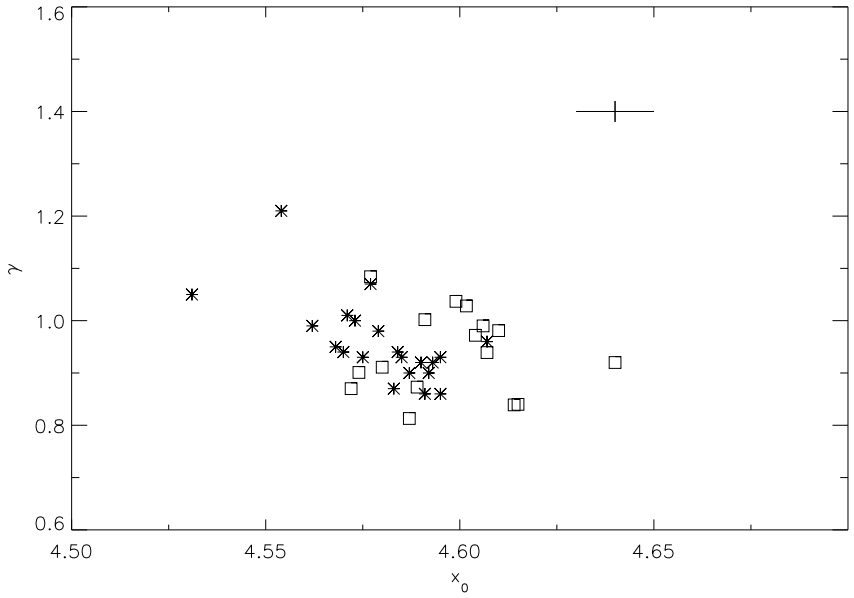

Figure 3.10: FM parameters x_0 and γ in HII regions. Stars: JG93's parameters for stars in HII regions from Aiello et al.'s (1988) sample. Squares: the parameters for the same stars in the database. The representative error bar indicates the typical uncertainty in both samples.

results could be confirmed – HD 29647 does seem to have a (barely) shifted bump.

The extinction toward HD 62542 has long been believed to have a shifted bump (Cardelli & Savage 1988). However, this is not seen in its extinction curve here, with $x_0 = 4.54 \pm 0.03$. Cardelli & Savage (1988) found $x_0 = 4.74 \pm 0.03$, and in the extinction curve shown in their work, the bump is visibly shifted blueward. In an effort to reproduce their results, the same IUE spectra and UV comparison star as used by Cardelli & Savage (1988) were used to construct an extinction curve. This curve was then fit over three ranges; the original FM90 range (3.3 - 8.7 μm), from 3.7 - 8.0 μm , and

from 3.7 - 8.7 μm excluding the region around Lyα. None of these ranges produced a shifted bump.

The remaining differences were in the reddened IUE spectra themselves. While the spectra used by Cardelli & Savage (1988) are the same as used here, their spectra were reduced with a different software package, IUE-SIPS, than those in the final archive, NEWSIPS. (NEWSIPS-reduced spectra did not become available until the mid 1990s.) The main improvement in NEWSIPS-reduced, low dispersion spectra is the 10 to 50% increase in the signal-to-noise. However, the line libraries used to find the dispersion during wavelength calibration were also expanded, with the result being better sampling of the dispersion and more accurate wavelength calibration (Nichols & Linsky 1996).

Only one sightline was shifted nearly 3 σ beyond the mean (4.59$\pm$0.01), HD 29647 ($x_0 = 4.70 \pm 0.03$), but the lack of significance of the shift was worrisome, especially in light of the lack of a shift in HD 62542's bump. Cardelli & Savage (1988) found $x_0 = 4.70 \pm 0.03$ for HD 29647, the same as found here. Values of x_0 were found using the three other fitting ranges that were considered when testing for HD 62542's bump shift. The values of x_0 that were found were all easily within 1 σ of the mean, and the values of x_0 found over all three ranges are within 2 σ of each other. Thus, it is quite possible that HD 29647's bump also is not shifted.

To further emphasize the likelihood of HD 29647's bump not being shifted, another sightline that passes through the same cloud, HD 283809, is considered. It, too, shows the water ice feature at 3.07 μm, as well as a weak

Table 3.3: Deviations of Non-CCM Sightlines

HD/BD	$\delta(4.65)$	$\delta(4.90)$	$\delta(5.07)$	$\delta(5.24)$	$\delta(7.82)$
29647	-0.58	-0.35	-0.18	-0.08	0.31
62542	-1.49	-1.10	-0.75	-0.50	1.12
204827	-0.65	-0.44	-0.29	-0.18	0.43
210121	-2.63	-2.35	-1.76	-1.24	2.33

3.4 μm feature (Gordon et al. 2003, in preparation) attributed to CH in the diffuse ISM (Pendleton et al. 1994). However, its bump, though weak ($c3/R_V$=0.43±0.08) is not shifted, as x_0 = 4.63±0.01. Whittet et al. (2003) showed that the bump carrier is likely found in the diffuse material around the dark cloud by finding the "difference curve" between two sightlines toward the Taurus Dark Cloud (hereafter TDC). This was done by subtracting the unnormalized extinction curves of HD 283809, whose extinction was assumed to be a blend of dark and diffuse components, from that of HD 283800, whose extinction curve is dominated by diffuse cloud extinction local to the outer portions of the molecular cloud, though it is also associated with the TDC. Both sightlines were assumed to have similar diffuse outer-cloud extinction components. The difference curve, believed to show the extinction due to the molecular cloud, had no bump whatsoever. By combining these dark/diffuse components in different amounts, Whittet et al. (2003) were aas ble to produce a curve that was a reasonable fit to HD 29647's extinction curve. This emphasizes the possibility that the bump carrier is found in diffuse regions, and processing in dark clouds destroys it (or at least, alters it significantly). If this is truly the case, then there is no reason to expect the bump to shift in dark regions.

According to Hecht (1986), a lack of correlation between x_0 and γ could be explained if the carrier is small graphite grains, for which $\gamma \propto 1/a$, where a is the grain radius, while x_0 is not a function of size (Bohren & Huffman, 1983). Hecht (1986) concluded that some fraction of small ($a < 50$Å) carbonaceous grains are bare, though possibly some have impurities; these are responsible for the bump. In this scenario, the bump width is dependent on the temperature and size distribution of these grains. The remaining small carbon grains retain their hydrogen, which would suppress the bump (Hecht 1986). One objection to this was that it required an overabundance of small grains in dense regions relative to diffuse regions (FM86; Sorrell 1990), since a large value of γ implies small grain size in this scenario. This conflicted with the observation that dense regions tend to have higher values of R_V, indicating the prevalence of large grains. However, the results of CCM, confirmed here, show that x_0 is not dependent on R_V (or anything else); thus, the grains which produce the bump form a separate population from those which are responsible for variations in R_V (CCM). On the other hand, it can be seen in Fig. 3.4 that there is a weak correlation between γ and R_V^{-1}. This agrees with the finding that γ is environment dependent. In 1990, Sorrell expanded upon Hecht's (1986) work; instead of temperature and size distributions influencing the bump width, he suggested the accretion of hydrogen on larger graphite grains with 60 Å$< a <$ 80 Å were responsible. He argued that might account for the width's environmental dependence, with H atoms forming mantles on grains in dense regions and thus broadening the

bump, without affecting x_0 (Sorrell 1990). However, while grains facilitate the formation of H_2 in clouds, they cannot form mantles (Spitzer 1978).

Mathis (1994) compared different mantle materials and their modeled bump attributes to observed bump attributes in order to determine the most likely mantle materials. This was done using the standard optical constants of Draine & Lee (1984) and Draine (1985, 1987) for graphite, and optical constants for the mantling material from various sources. He considered diamond, amorphous carbon (AMC), water ice, and PAH mantles on graphite cores. He found that the diamond coating tended to shift x_0 to longer wavelengths; a thin mantle would shift x_0 to 4.47, well below what has been observed. A coating of amorphous carbon does not fit the findings much better, as a thin mantle yields x_0 =4.57 but a low γ= 0.84. Increasing the thickness of mantle does not increase γ to values that are observed; a thicker mantle only broadens the bump to γ=0.93. Hydrogenated amorphous carbon mantles are even less suitable, as these shift x_0 to longer wavelengths while having even less of an impact on γ than AMC did. Water ice mantles may broaden γ, but only two sightlines (HD 29647 and HD 283809) have the telltale 3.07 μm ice feature. It is possible that there are mantles that are thin enough that they produce only a very weak feature but Warren (1984) showed that ice mantles do not affect the bump because there is almost no absorption at wavelengths near 2175 Å. Neutral PAHs are a more likely candidate, as they can produce both x_0 and γ consistent with observations, with $x_0 \approx 4.61$ for γ= 1.0. However, this was found by assuming that the optical constants of isolated PAHs are similar to those comprising the mantle and

by igoring impurities which might alter the PAH optical properties. Another drawback is that neutral PAHs have an absorption feature near x=3 which is not seen, though Joblin et al. (1992) showed that this could be masked by averaging over a distribution of PAHs of different sizes. Also, it is unlikely that many PAHs are neutral in the diffuse ISM (LePage et al. 2003), though Verstraete et al. (1990) claims that most should be neutral in cool clouds. A recent search for the effects of small PAHs ($\approx$ 30 - 50 C atoms per molecule) on UV extinction concluded that they probably do not play a large role (Clayton et al. 2003), as small PAHs seem to be destroyed easily (Allain et al. 1996; LePage et al. 2003), though it is still possible that larger PAHs contribute. Thus, it seems that PAHs may be the most likely candidate for mantle materials, despite the problems outlined above.

3.2 Adherence to the CCM Relation

This section demonstrates that the vast majority of sightlines follow the CCM relation.

In 1988-1989, Cardelli, Clayton, & Mathis (CCM) published their findings that the shape of the UV extinction curves could, for the most part, be described by the parameter R_V, which was in turn dependent on IR and B- and V-band photometry. This was significant for several reasons. First, the results of CCM implied that the physical and chemical processes which modify grains affect them efficiently and across entire distributions of grain compositions and sizes, as changes to the extinction at one wavelength are accompanied by changes in the entire average curve. Second, it showed that

variations in UV extinction curves tend to behave in a coherent, predictable way, thus allowing for more accurate dereddening than just removing the Galaxy average extinction curve (which corresponds to R_V=3.1). Third, CCM provided a better context in which to compare sightlines; previously, extinction was considered with respect to the Galactic average curve. However, the set of curves used at the time to make the average was slightly biased toward regions with extreme extinction properties, as such regions would have unusual sightlines. Thus, the average of such a set may not be representative of the Galaxy at large (Fitzpatrick 1999). Indeed, it has been shown that many lines of sight that have previously been considered "anomalous" when compared to the Galactic average are not anomalous at all but have a different value of R_V (Fitzpatrick 1999). Thus, the Galactic average is not a useful concept when considering extinction curves, as it does not reflect the physical processes occuring along a sightline. This illustrates that the CCM relation provides not a Galactic average curve, but an average curve for a specific value of R_V. Fourth, not all Galactic sightlines adhere to the CCM relation. This implies the existence of an unusual environment local to the dust. Studying sightlines that do not follow the CCM relation can shed light on the processes that modify grains and perhaps yield a better understanding of the nature of the grains themselves.

3.2.1 Deviations from CCM

In order to determine which sightlines followed CCM and which did not, a method similar to that used by Mathis & Cardelli (1992; hereafter MC92) was used here. MC92 looked for patterns in sightlines' deviations from CCM

which might shed light on either the grain composition, environment dependence, or both. In other words, if the deviation from CCM at a certain wavelength is known, what can be said about the deviations at other wavelengths? To answer this, they first separated the CCM sample into three groups depending on the environment: sightlines that pass through dark clouds, bright nebulosities, or neither. For each sightline, the deviation from CCM was calculated to be simply the difference between the extinction curve and the CCM curve, both normalized to A(V); see Eq. 3.1. To relate this to the deviation at specific wavelength,

$$\delta(x_i) = [A(\lambda)/A(V)]_i - [A(\lambda)/A(V)]_{CCM} \tag{3.1}$$

MC92 found that there is a difference in the shape of the deviations of the FUV rise through dark clouds and bright nebulae. They also found that for bright nebulae, the deviations occur selectively near the central wavelength of the bump.

The sightlines in the sample used here were fit with a CCM curve using a standard IDL curve fitting routine that minimized the χ^2. The values of R_V found this way were compared to those calculated using IR photometry; this is shown in Fig. 3.11. A line with slope unity and zero intercept is overlayed for comparison. While there is scatter about the line, there is generally fair agreement between the two values, with the fitted R_V being within 3σ of the calculated value for 93% of the sample. In Fig. 3.11, error bars have been placed on values beyond 3σ, and the sightlines to HD 210121, HD 204827, HD 29647, and HD 62542 are indicated.

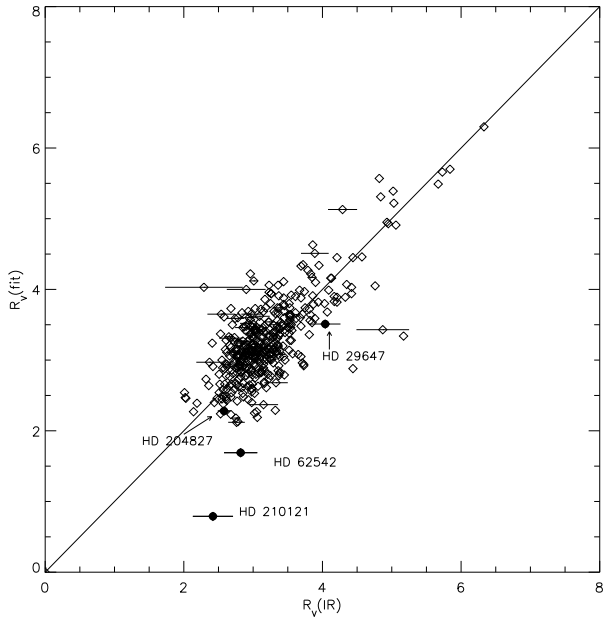

Figure 3.11: Comparison of the fitted R_V values and the R_V values found with IR photometry. For contrast a line with a slope of unity has been overlayed. 1σ error bars are shown for those more than 3σ from the mean.

One thing to consider when fitting R_V is that there are two different kinds of deviations from CCM. There are sightlines which deviate like the Magellanic Clouds, which cannot be fit with any CCM curve, and there are those which are not well fit by their R_V curve, but can still be fit with a CCM curve of different R_V. Thus, fitting an extinction curve to find R_V can actually yield an incorrect value of R_V, since the underlying assumption – the best fit will always give an R_V value similar to the "real", measured R_V– is not valid in all cases. To demonstrate, HD 210121 is behind a high latitude translucent cloud and is known to have an unusual extinction curve (Larson et al. 1996) with very strong FUV extinction. It has a measured R_V of

2.42±0.29, but is not well fit by the corresponding CCM curve. Its best fit is R_V=0.76, which is significantly different from the IR-derived value. Despite this caveat, the vast majority of sightlines (93%) had fit R_V values that were within 3 σ of their calculated R_V. This is surprising, as it indicates that the vast majority of sightlines follow the CCM relation closely. Sightlines that had fit R_V values beyond 3 σ from their calculated R_V values were flagged for further investigation.

Plots which compare the deviations between the FM parameter curves and the best-fit CCM curves at different wavelengths (x=4.65, 4.90, 5.07, 5.24, 7.82) were examined to find trends between deviations from CCM, density A(V)/distance, and environment. With the exception of the last wavelength (x = 7.82), these are the same as those selected by MC92 and were chosen specifically to facilitate comparisons between MC92's results and those derived here. MC92 selected x = 8.0 as one of their comparison wavelengths. As this was the short wavelength cutoff for the extinction curves in this database, a slightly longer wavelength was used. The uncertainty, which came primarily from the uncertainty in the FM fit, was often large compared to the deviations. The mean deviation and its uncertainty at the five wavelengths mentioned above was found. Sightlines that were beyond 3 σ from the mean at any of the five wavelengths were flagged for further consideration. The deviation plots are in Fig. 3.12; the outlying sightlines are named, and error bars are shown for sightlines that deviate significantly from the mean.

Table 3.4: Comparison Between Fitted and Calculated R_V Values

HD/BD	R_V(IR)	$\sigma_{R_V(IR)}$	R_V(fit)
29647	4.04	0.22	3.51
62542	2.82	0.24	1.71
204827	2.58	0.09	2.28
210121	2.42	0.29	0.76

Sightlines were considered potentially non-CCM if they had either significant differences between their fit and calculated R_V values or significant deviations between their extinction curves and their best-fit CCM curves. All such sightlines were investigated further to see if they truly were non-CCM like by comparing their extinction curves to their calculated R_V curves. The literature was searched for information about anything which might suggest unusual grain processing along the sightlines. The two curves were similar in shape and within 2 σ of each other for all sightlines except for the four anomalous ones that were known previously, HD 210121, HD 204827, HD 62542, and HD 29647, which are deviant at several wavelengths. The four sightlines are shown in Fig. 3.13, along with HD 283809; the solid line is the extinction curve itself and the dash-dotted line is the CCM curve for the fit R_V. Their deviations at various wavelengths are listed in Table 3.3 and both their fitted and calculated R_V values are in Table 3.4. HD 62542, HD 210121, HD 204827, and HD 29647 are considered below. HD 204827 is discussed in more detail in the next chapter.

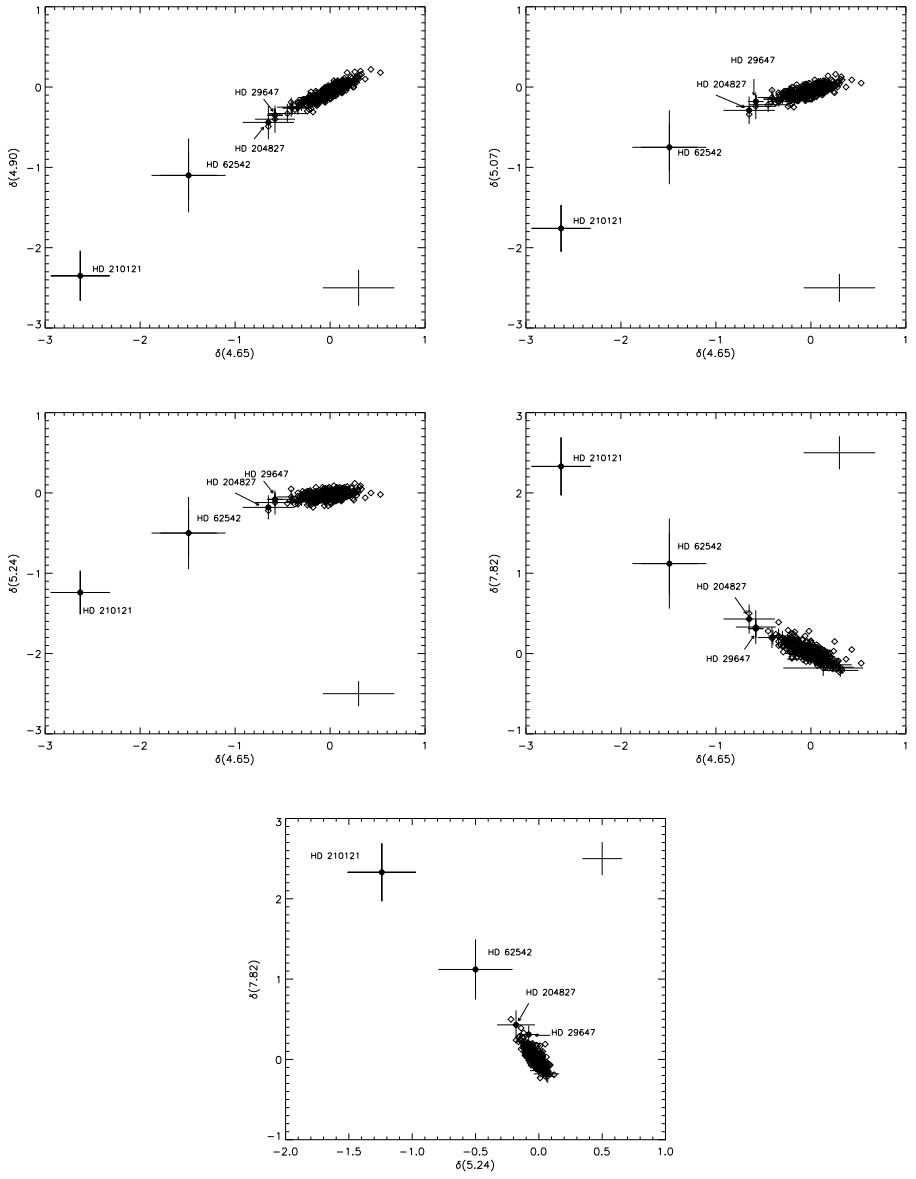

Figure 3.12: Deviation plots at the wavelengths $x = 4.65, 4.90, 5.07, 5.24$, and 7.82. 1σ error bars are shown for non-CCM sightlines and those which are beyond 3 σ from the mean. Also, representative 1σ errors bars are shown.

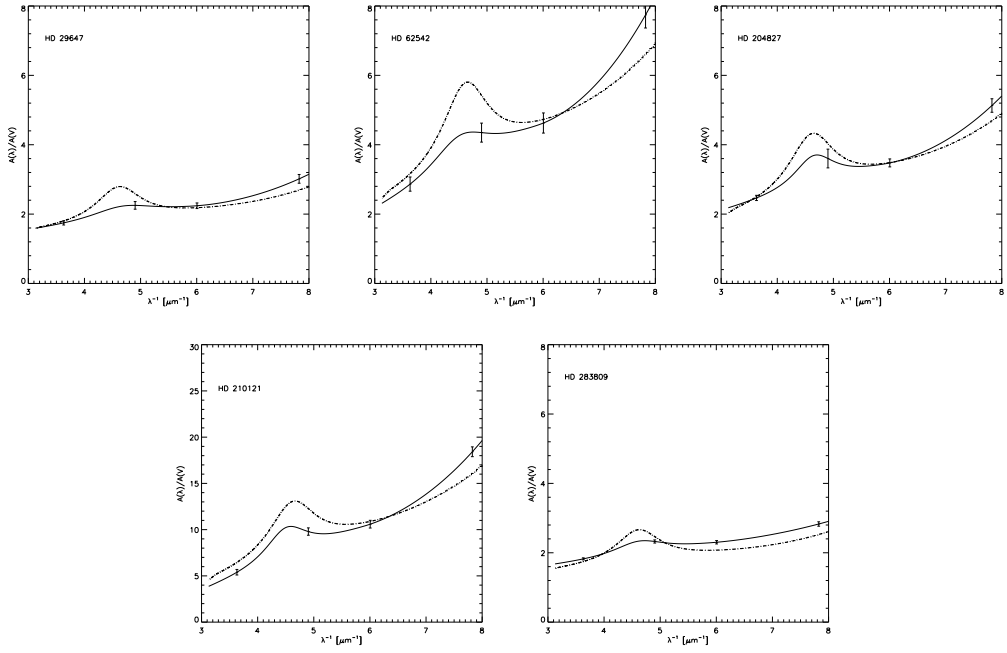

Figure 3.13: The extinction curves of nonCCM sightlines. HD 283809, while not in the database, is included for the sake of comparison.

3.2.2 The Non-CCM Sightlines

The apparent lack of non-CCM sightlines in the Galaxy could be attributed to two things: 1.) the IUE archive dataset favors lines of sight through more or less "normal" environments; 2.) the physical processes that are the underpinning of the CCM relation which govern grain modification hold along almost every sightline that has been observed. These possibilities are considered below.

First, IUE was sensitive to about 15^{th} mag for low dispersion spectra, and was often used for studies of the ISM. In this work, only bright sightlines were considered; the faintest stars have V $\approx$ 11. This differs from the instrumental faintness limit because the stars considered here were reddened, and as UV light is preferentially extinguished compared to light of longer wavelength, the IUE spectra for heavily reddened, faint sightlines often had low signal-to-noise ratios. This faintness limit in and of itself is a factor, as heavily extinguished objects could not be observed. Thus, there is little information on grain processing in dark clouds. However, virtually all of the non-CCM sightlines known today are in the (diffuse) Magellanic Clouds, not in dense Galactic clouds. It is worth noting that out of 426 sightlines, only 4 (HD 210121, HD 204827, HD 29647, HD 62542) deviated consistently from CCM. In contrast, Clayton et al. (2000), found that out of a sample of 26 Galactic stars along low density, low reddening sightlines, 7 sightlines could be averaged to find an extinction curve very similar to the LMC. These 7 stars were found to be behind gas that showed signs of being subjected to shocks. Thus, while IUE's sensitivity certainly influenced the selection of stars to

be brighter and less extinguished, there is evidence that non-CCM sightlines favor less dense, harsher environments.

HD 204827 is an intriguing sightline; it will be shown in the following chapter that its partially dereddened curve resembles that of the SMC, even though the environment of the dust in the HD 204827 cloud is quite different from that seen in the SMC sightlines. The column density of the dust (E(B-V)=0.55 mag) in the HD 204827 dust cloud is larger but the cloud also has a much higher density. The HD 204827 dust cloud resembles a molecular cloud more than the diffuse ISM. The HD 204827 cloud is very rich in carbon molecules, showing large column densities of C_2, C_3, CH, and CN (Oka et al. 2003; Thorburn et al. 2003). In this respect, the HD 204827 cloud dust is quite similar to the sightline toward HD 62542 (Cardelli & Savage 1988). This sightline shows a severely non-CCM sightline with a broad bump and steep far-UV extinction. Its dust is also rich in carbon molecules. The projected position of HD 62542 lies on the edge of material swept up by a stellar wind bubble. Three other non-CCM, weak bump, steep far-UV sightlines in the Galaxy, HD 283809, HD 29647, and HD 210121, are also associated with dense clouds (Cardelli & Savage 1988; Larson, Whittet, & Hough 1996; Cardelli & Wallerstein 1989; Gordon et al. 2003). The dust in the molecular cloud associated with HD 210121 is likely to have been processed as it was propelled into the halo during a Galactic fountain or other event. The other two sightlines toward HD 29647 and HD 283809 seem to be sampling dust in quiescent dense clouds. These two sightlines show a strong 3.07 μm ice feature. They also show a weak 3.4 μm feature

similar to the one seen in the HD 204827 cloud dust (Goebel 1983; Smith, Sellgren, & Brooke 1993). The steep far-UV extinction in these clouds helps shield the molecules in these clouds from dissociating UV radiation leading to larger column densities than might be found in clouds with less steep far-UV extinction (Mathis 1990). To illustrate, Fig. 3.14 shows the deviation $\delta(7.82)$ compared to the density of CN along the sightline. CN can be used as an indicator of relatively dense regions in diffuse, molecule-rich clouds (Joseph et al. 1986; Gredel et al. 2002). CN column densities for 46 sightlines, including the four non-CCM sightlines discussed above, are from Federman (1994) and Oka et al. (2003). The average $\delta(7.82)$ and N(CN)/A(V)(10^{13}cm^{-2} mag^{-1}) for the CCM-like sightlines were 0.03±0.03 and 0.33±0.01, respectively; for the non-CCM sightlines, these values were 1.06±0.15 and 2.75±0.15. Thus, it can be seen that these four sightlines have both high N(CN)/A(V) and sigificant deviation from CCM at x=7.82 compared to the CCM-like sample. As mentioned previously, this is an interesting contrast when compared to the Galactic non-CCM sightlines of Clayton et al. (2000) and those in the Magellanic Clouds. The Milky Way sightlines which resembled those toward the LMC were all in the same area and passed through gas which is believed to have been subjected to shocks. The gas-to-dust ratio was found to be consistent with the Galaxy average. In Chapter 4, it will be shown that the CCM-like ISM in front of HD 204827, a sightline with a weak bump and strong FUV extinction, can be removed, thus revealing dust along a high density Milky Way sightline that can mimic the extinction properties of SMC-type dust. Again, this dust had been exposed to strong OB winds or a

supernova shock. The gas-to-dust ratio for the HD 204827 sightline could not be found, but the metallicity of its OB association was comparable to that of other Galactic B stars (Daflon et al. 1999). This instance of Magellanic Cloud-type dust in the Milky Way supports the conclusion of Clayton et al. (2000) that the local environment may be a more influential factor than global ISM properties (such as metallicity and gas-to- dust ratio) when it comes to extinction properties. These two sightlines can be seen in the bottom panel of Fig. 3.15. The similarities between the SMC Bar extinction curve in the top panel of Fig. 3.15, and the partially dereddened Galactic sightline, and the LMC2 Supershell extinction curve and the non-CCM sightline average of Clayton et al. (2000), are clear.

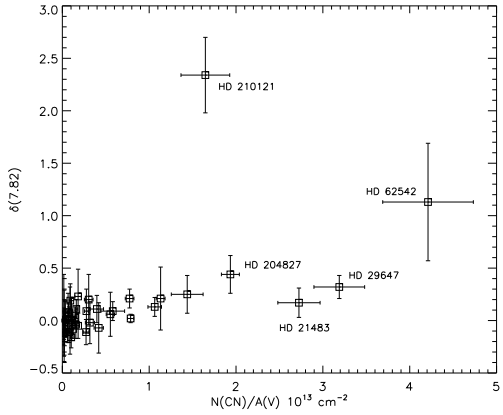

Figure 3.14: The deviation at 7.82 μm^{-1} vs. the density of CN.

Several things can be said about non-CCM sightlines as a group.

(1.) It is worth emphasizing again that there are very few of them. Out of 426 sightlines, only 4 deviated consistently from CCM by more than 3 σ.

This suggests that the grain processing which results in CCM-like extinction dominates the ISM.

(2.) These sightlines are relatively dense, and rich in molecules.

(3.) They tend to have weak bumps and strong FUV extinction for their measured R_V CCM curves, especially those which pass through cold, quiescent regions. The two sightlines through the TDC, HD 29647 and HD 283809, show this well. The weakened bump may reflect processing which modifies or destroys the bump carrier in dark clouds (Whittet et al. 2003).

(4.) Other dense sightlines with strong FUV extinction, HD 204827, HD 62542, and HD 210121, pass through dense clouds that may have been exposed to shocks or strong UV radiation that disrupt large grains, possibly resulting in a size distribution that is skewed toward small grains.

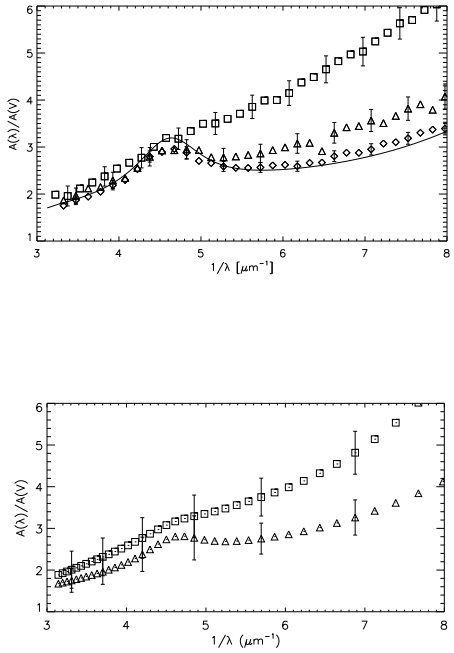

Figure 3.15: Top: Extinction curves of the average LMC (diamonds), LMC2 Supershell (triangles), SMC Bar (squares), and CCM R_V=3.1 (solid line). Bottom: HD 204827's partially dereddened sightline (squares; see Chapter 4) and the diffuse, non-CCM Galactic curve from Clayton et al. (2000) (triangles).

4. SMC-Type Dust in the Milky Way

(A paper based on this chapter is in press in the Astrophysical Journal.)

The CCM average Milky Way extinction relation, A_λ/A_V, is applicable to a wide range of interstellar dust environments, including lines of sight through diffuse dust and dark cloud dust, as well as dust associated with star formation. However, the CCM relation does not usually apply beyond the Milky Way, even in other Local Group galaxies such as the Magellanic Clouds and M31 (e.g., Clayton & Martin 1985; Fitzpatrick 1985, 1986; Clayton et al. 1996; Bianchi et al. 1996; Gordon & Clayton 1998; Misselt, Clayton, & Gordon 1999). There is some evidence that it may apply along some sightlines in the Large Magellanic Cloud (Gordon et al. 2003). It is important to understand why dust in these other galaxies is different since many extragalactic environments seem to contain interstellar dust that is better represented by dust in the SMC than the Milky Way (e.g., Gordon, Calzetti, & Witt 1997; Pitman, Clayton, & Gordon 2000). Real deviations from CCM are seen for a few sightlines in the Galaxy (Cardelli & Clayton 1991; Mathis & Cardelli 1992). Sightlines such as those toward HD 62542, HD 204827, and HD 210121 show weak bumps and anomalously strong far-UV extinction for their measured values of R_V. Other steep far-UV, weak bump dust was found along some low density, low extinction sightlines (Clayton, Gordon, & Wolff 2000). The extinction along these sightlines resembles those seen in the LMC but none approach the extreme properties of the SMC sightlines. Nevertheless, studying these anomalous Galactic sightlines may

be a key to relating the differing extinction characteristics to various dust environments seen in the Milky Way and other galaxies.

The ultraviolet extinction properties of dust toward 18 stars in Trumpler 37, including HD 204827, were studied more than 15 years ago (Clayton & Fitzpatrick 1987, hereafter CF). At that time, the UV extinction, in this region of the sky, was referred to as anomalous as it was generally steeper than the average Galactic extinction curve. This extinction in the Trumpler 37 region is no longer considered anomalous. The extinction curves, with one exception, fit the CCM relation with R_V values less than the Galactic average of 3.1. The exception is HD 204827, which has an extinction curve significantly steeper than the appropriate CCM curve.

In this work, we take advantage of improved IUE data along with infrared data from 2MASS and IRAS to re-investigate the dust associated with HD 204827 and Trumpler 37.

4.1 UV Extinction Curves

IUE spectra for all eighteen stars in Trumpler 37, previously studied by CF, were obtained from the Multimission Archive at Space Telescope (MAST). The archive spectra were reduced using NEWSIPS and then recalibrated using the method developed by Massa & Fitzpatrick (2000). The signal-to-noise of the NEWSIPS IUE spectra has been improved by 10-50% over that used by CF (Nichols & Linsky 1996). Low dispersion LWR/LWP and SWP spectra were selected, from either aperture. Multiple spectra from one camera were averaged and then the long and short-wavelength segments were

Table 4.1: IUE Spectra and Photometry Sources of Program Stars

HD/BD	SWP	LWP/LWR	UBV Source
204827	11131, 14530	09761, 11104	1
205794	23119	03451	2
205948	23122	03453	2
206267	26011	06057, 17971	2
239683	23130	03460	2
239689	23138	03466	2
239693	23131	03463	2
239710	17470	13757	2
239722	23125	03456	3
239724	23118	03450	2
239725	23136	03464	2
239729	13451	10114	2
239738	23123	03454	3
239742	23129	03459	4
239745	23128	03458	2
239748	23137	03465	4
+57 2395B	23132	03461	3
+58 2292	23139	03467	3

NOTE. – (1) Hiltner 1956, (2) Nicolet 1978, (3) Garrison & Kormendy 1976, (4) Simonson 1968. All JHK photometry is from 2MASS.

merged at the shortest wavelength of the SWP. The wavelength coverage is ∼1200 – 3200 Å. The sample stars and their IUE spectra are listed in Table 4.1.

The standard pair method, in which a reddened star is compared with an unreddened one of the same spectral type, was used to construct each sightline's extinction curve (Massa, Savage, & Fitzpatrick 1983). The unreddened comparison stars were selected from Cardelli, Sembach, & Mathis (1992), which were drawn from the IUE spectral atlas of Wu et al. (1983). The spectral matches were made on the basis of comparing the UV spectra of

pairs of stars rather than matching their visible spectral types. R_V was estimated from the JHK colors as described in Fitzpatrick (1999). A_V was found using R_V and E(B-V). The extinction curves are normalized to A_V. Table 4.1 lists the sources of the UBV photometry. Photometry in the JHK bands was available for all the stars in the sample from the 2MASS database (Cutri et al. 2003). Table 4.2 lists the spectral type, reddening, and calculated R_V for each star in the sample. In general, our UV spectral classifications are in good agreement with those of CF. The resulting extinction curves were fit with the Fitzpatrick-Massa (FM) parameterization (Fitzpatrick & Massa 1990). The fit has been limited to the wavelength range 2700 – 1250 Å (3.7-8.0 μm^{-1}), as it is not reliable longward of 2700 Å (E. Fitzpatrick 2002, private communication), and the 1250 Å cut-off excludes the Lyα feature at 1215 Å. The normalization of the FM parameters was converted from E(B-V) to A_V. The parameters are listed in Tables 4.3 and 4.4. In Figure 4.1, the extinction curve and corresponding CCM curve for each sightline are shown.

The Cep OB2 association is a complex system with several distinct regions. Previous studies have placed it at a distance of around 800 pc (e.g., Garrison & Kormendy 1976; Georgelin & Georgelin 1976) though an analysis of Hipparcos parallaxes have placed Cep OB2 much closer, at 615 pc (de Zeeuw et al. 1999). Most of the stars in our sample are probably members of the Trumpler 37 association (Marschall & van Altena 1987; de Zeeuw et al. 1999). The possible exceptions are HD 239724, which has been placed at about 3 kpc (Simonson 1968) and HD 204827, placed at about 500 pc (CF). However, de Zeeuw et al. (1999) give a probability of 66% that HD

Table 4.2: Properties of Program Stars

HD/BD	Sp Type	UV Sp Type	E(B-V)	R_V
204827	B0 V	B0 V	1.10±0.05	2.58±0.12
205794	B5 V	B0.5 V	0.62±0.05	3.09±0.26
205948	B2 V	B1 V	0.50±0.04	2.90±0.27
206267	O6 V	O7 V	0.52±0.04	2.82±0.22
239683	B5 V	B2 IV	0.54±0.04	2.76±0.22
239689	B5 V	B1 V	0.45±0.04	2.70±0.29
239693	B5 V	B4 IV	0.41±0.04	2.37±0.27
239710	B3 V	B1 V	0.62±0.07	3.02±0.32
239722	B5 V	B1 V	0.93±0.05	2.86±0.17
239724	B1 III	B1.5 III	0.62±0.04	3.18±0.24
239725	B5 V	B1 V	0.52±0.04	3.14±0.28
239729	B0 V	O9 V	0.66±0.04	3.19±0.19
239738	B5 V	B2 V	0.51±0.05	2.90±0.32
239742	B5 V	B4 IV	0.38±0.04	2.36±0.31
239745	B5 V	B1.5 V	0.54±0.07	2.66±0.34
239748	B5 V	B1 V	0.43±0.04	2.93±0.31
+57 2395B	B5 V	B2 V	0.64±0.04	2.44±0.19
+58 2292	B5 V	B2 V	0.57±0.03	3.00±0.26

204827 is a member of Cep OB2, and Marschall & van Altena (1987)give a 93% probability that HD 239724 is a member of Trumpler 37. The distance to HD 204827 is uncertain since it is a spectroscopic binary (Petrie & Pearce 1961; Mason et al. 1998).

With the exception of HD 204827 and HD 239722, the reddenings of all the sample stars lie between E(B-V) of 0.4 and 0.6 mag. This reddening is primarily due to dust foreground to Trumpler 37. Using the average reddening per kpc in the Galaxy, we would expect 0.4-0.5 mag in front of Trumpler 37 if it lies at a distance of 600-800 pc (Spitzer 1973). Therefore, only the sightlines toward HD 204827 (E(B-V) = 1.10) and HD 239722 (E(B-

V)=0.93) seem to contain significant amounts of additional dust that may be associated with Trumpler 37 itself.

The calculated values of R_V for the sample stars tend to be smaller than 3.1 although almost all the estimated R_V values are within 2σ of 3.1. Averaging the sixteen stars in the sample having low to moderate reddening, we get E(B-V) = 0.53±0.01 mag and R_V = 2.84±0.07. As can be seen in Figure 4.1, with the exception of HD 204827, none of the Trumpler 37 extinction curves deviates more than 2σ from its corresponding CCM curve. The dust foreground to the Trumpler 37 appears to be normal diffuse interstellar dust adhering to the CCM relation.

In an effort to separate the effects of the foreground dust and dust local to the cloud, we partially dereddened the IUE spectra and UBVJHK photometry for HD 204827 and HD 239722. A CCM-type extinction corresponding to E(B-V)= 0.55 mag and R_V = 2.84 was removed. Extinction curves were then recalculated for these two sightlines using these partially dereddened spectra, their corrected colors, and their original UV comparison spectra. The residual reddening toward HD 204827 from Trumpler 37 dust is E(B-V) ∼0.55 mag and toward HD 239722 it is E(B-V) ∼0.4 mag. The new HD 239722 curve is not significantly different from the original curve with the foreground included. They differ by only $\sim 1\sigma$. However, the new HD 204827 curve is significantly different, as shown in Figure 4.2. It is now extremely steep and has almost no 2175 Å bump. In fact, it is indistinguishable within the uncertainties from the average SMC bar extinction curve (Gordon et al.

2003). This has also been plotted in Figure 4.2. The two curves lie within 1σ of each other.

The FM parameters for HD 204827's partially dereddened curve were also found. These are listed in Tables 4.3 and 4.4, as are the average values for the SMC Bar (Gordon et al. 2003). They were found with the same method Gordon et al. (2003) used to find FM parameters for the SMC Bar sightlines. This required holding x_0 and γ fixed at 4.60 and 1.00, respectively, while varying the other parameters such that χ^2 was minimized. Again, these values are within each other's uncertainties.

4.1.1 IR Emission

Figure 4.3 shows $0.5^\circ \times 0.5^\circ$ IRAS HiRes images centered on HD 204827 in the 25 and 60 μm bands (Aumann, Fowler & Melnyk 1990). IRAS HiRes images have spatial resolution better than $1'$ and fluxes good to 20%. HD 204827 shows an apparent bow shock in the 25 and 60 μm images (van Buren & McCray 1988). Integrated fluxes in Janskys were found over a square aperture of $25'$ on each side. The background flux was also found and removed. The measured fluxes are listed in Table 4.5, along with the color temperatures T_d estimated from the flux ratios (Ward-Thompson & Robson 1991). These are similar to T_d in bow shocks found elsewhere (Ward-Thompson & Robson 1991; van Buren & McCray 1988). We also fit the IRAS fluxes with a blackbody curve. A temperature of $\sim$75 K yielded the best fit for the data.

Bow shocks are generally associated with early-type runaway stars having

peculiar space velocities in excess of 30 km s^{-1} (Blauuw 1961). Using the observed radial velocity of HD 204827 (Gies 1987) and its Hipparcos proper motions, we calculate the peculiar space velocity $v_{space}^{pec} = 35.1 \pm 25.2$ km/s. Since the uncertainty in the velocity is rather large, we can only say that the velocity of HD 204827 is consistent with being a runaway star. The standoff distance of the HD 204827 bow shock (4.5′ or 0.9 pc at a distance of 650 pc) seen in Figure 4.3 is also consistent with this velocity and the standard assumptions made in Van Buren & McCray (1988).

4.1.2 IR Spectroscopy

In 2001 and 2002 August, IR spectra of HD 204827 and HD 239722 (the other highly reddened cluster member) were obtained with the SpeX instrument at the NASA Infrared Telescope Facility (IRTF). SpeX is a medium resolution spectrograph which can cover a wavelength range from 0.8 to 5.5 μm. For this investigation, the 1.9-4.2 μm, cross-dispersed mode was used. These data were reduced using version 2.0 of the associated SpexTool software (Cushing, Vacca, & Rayner 2003; Rayner et al. 2003). To remove telluric lines, the spectrum of a ratioing G star was obtained at the same time, with observations bracketing those of the program star. The difference in airmass between the target and the G star averaged 0.02 and they were separated by less than one degree on the sky. The reduced target spectrum was then multiplied by a solar spectrum scaled to match the G star so that the stellar lines introduced by the division would be removed. The resulting spectrum then had a blackbody curve removed, corresponding to the effec-

tive temperature of the UV spectral classification. Optical depth plots were then derived following the method of Sandford et al. (1991), by fitting and removing a linear baseline to the reduced spectrum between 3.23 and 3.64 μm. For HD 204827, the C-H feature's optical depth was then measured at 3.42 μm (Pendleton et al. 1994), yielding $\tau_{3.4} = 0.0139 \pm 0.0036$.

HD 204827's optical depth plot is shown in Figure 4.4 (top), overlayed with the spectrum of the Murchison meteorite (de Vries et al. 1993) and a zero line for easier comparison. The 3.4 μm aliphatic C-H stretch is weak, but present. The middle panel of Figure 4.4 shows the optical plot with the scaled Murchison spectrum subtracted for emphasis. This feature arises from an organic carrier in the diffuse ISM. Pendleton et al. (1994) used a sample of sightlines, with $A_V \geq 3.9$ mag, to show that there is a correlation between A_V and the feature's optical depth $\tau_{3.4}$, with the average value of $A_V/\tau_{3.4} = 270 \pm 40$ in the diffuse ISM. Our value of $A_V/\tau_{3.4} = 205 \pm 63$ is in agreement with their results. Thus, the sightline toward HD 204827 sets a new lower limit on the extinction ($A_V = 2.84 \pm 0.13$) at which the feature has been detected. There is no detectable 3.1 μm water ice feature (Pendleton et al. 1994 and references therein). HD 239722 does not show a significant 3.4 μm feature, with $\tau_{3.4} = 0.010 \pm 0.006$, though this sightline has a similar amount of extinction (A_V=2.66$\pm$0.18 mag) to HD 204827. Accordingly, HD 239722's $A_V/\tau_{3.4}$ (= 266$\pm$178) is not significant. Its spectrum is shown in Figure 4.4 (bottom), again with a zero line for contrast.

Table 4.3: Bump-Related FM Parameters of Program Stars

HD/BD	c_3/R_V	x_0	γ
204827	0.66±0.13	4.66±0.02	0.91±0.03
205794	1.05±0.19	4.57±0.01	0.88±0.02
205948	1.17±0.25	4.59±0.01	0.91±0.03
206267	1.02±0.20	4.59±0.01	0.91±0.03
239683	1.59±0.39	4.59±0.03	1.18±0.04
239689	1.29±0.18	4.57±0.005	0.96±0.02
239693	1.13±0.26	4.57±0.95	0.90±0.03
239710	0.71±0.18	4.60±0.02	0.82±0.03
239722	1.28±0.21	4.59±0.01	1.04±0.03
239724	1.07±0.19	4.60±0.01	0.94±0.03
239725	0.87±0.16	4.56±0.01	0.91±0.03
239729	1.01±0.16	4.61±0.01	1.08±0.03
239738	1.17±0.28	4.55±0.01	1.03±0.03
239742	1.84±0.58	4.58±0.02	1.03±0.04
239745	1.36±0.31	4.54±0.004	0.93±0.02
239748	1.08±0.25	4.57±0.01	0.88±0.03
+57 2395B	1.29±0.24	4.57±0.01	0.97±0.03
+58 2292	1.08±0.18	4.58±0.01	0.92±0.02
204827 (partially dereddened)	0.24±0.09	4.60±0.00	1.00±0.00
SMC Bar average	0.14±0.05	4.60±0.00	1.00±0.00

4.2 Discussion

The residual sightline toward HD 204827 with the foreground dust component removed is unique in the Galaxy. About 400 hundred sightlines in the Galaxy have measured UV extinction curves and no other sightline in the Galaxy shows an extinction curve resembling that seen in the SMC bar (Gordon & Clayton 1998; see Chapter 3). This includes the sightlines near to HD 204827 in the sky which are seen in Figure 4.1. So the HD 204827 sightline is sampling dust not seen along the nearby sightlines toward Trumpler 37 and

Table 4.4: Continuum-Related FM Parameters of Program Stars

HD/BD	c_1/R_V	c_2/R_V	c_4/R_V
204827	1.08±0.38	0.38±0.03	0.36±0.06
205794	1.27±0.40	0.17±0.03	0.14±0.04
205948	1.36±0.43	0.16±0.03	0.18±0.04
206267	1.17±0.45	0.27±0.04	0.22±0.05
239683	1.21±0.43	0.23±0.04	0.24±0.07
239689	0.84±0.27	0.28±0.04	0.18±0.03
239693	1.16±0.43	0.23±0.05	0.20±0.06
239710	1.56±0.49	0.15±0.04	0.20±0.06
239722	0.88±0.34	0.32±0.04	0.22±0.04
239724	1.09±0.35	0.21±0.03	0.14±0.03
239725	1.16±0.42	0.22±0.03	0.21±0.04
239729	1.11±0.25	0.22±0.02	0.25±0.04
239738	1.00±0.01	0.24±0.04	0.20±0.06
239742	0.57±0.33	0.38±0.11	0.15±0.07
239745	1.12±0.28	0.22±0.04	0.19±0.05
239748	1.21±0.41	0.20±0.04	0.25±0.06
+57 2395B	1.28±0.41	0.35±0.05	0.31±0.06
+58 2292	0.94±0.29	0.25±0.04	0.14±0.03
204827 (partially dereddened)	-1.85±0.54	0.82±0.15	0.11±0.04
SMC Bar average	-1.81±0.16	0.83±0.15	0.17±0.02

Cep OB2. For the purposes of this discussion, we shall refer to this dust as HD 204827 cloud dust. Using a similar method, Whittet et al. (2003) find a bumpless residual dust component but with a flatter UV extinction toward HD 283809 in the Taurus Cloud.

HD 204827 lies in the the outer part of the Trumpler 37 cluster, away from any bright rims or areas of nebulosity, north northwest of IC 1396. Its projected position also lies right on the edge of the Cepheus IRAS Bubble (Patel et al. 1998). The IRAS 100 μm image reveals that the position of

Table 4.5: IRAS Fluxes and Color Temperatures

Property	HD 204827
F(12μm) (Jy)	0.14±0.08
F(25μm) (Jy)	27.84±1.11
F(60μm) (Jy)	170.27±4.43
F(100μm) (Jy)	146.03±14.84
$T_{12/25}$ (K)	70±7
$T_{25/60}$ (K)	55±1
$T_{60/100}$ (K)	38±3

HD 204827 is projected on the edge of a peninsula of higher optical depth (Abraham, Balazs, & Kun 2000). The presence of the bow shock around HD 204827, indicates that the star may lie in or near the material swept up in the formation of the bubble. It formed through a combination of stellar winds and a supernova explosion from the first generation of star formation in the region, NGC 7160 which occurred about 7 Myr ago (Patel et al. 1998). The Trumpler 37 cluster formed about 5 Myr ago perhaps induced by the formation of the Cepheus Bubble. Shocks such as those in supernovae ejecta will produce a dust grain size distribution skewed toward smaller grains. This will lead to a steeper far-UV extinction but should also lead to a stronger 2175 Å bump since this feature is also believed to result from a population of small grains. (O'Donnell & Mathis 1997).

The four sightlines in the SMC that show extinction similar to that seen toward the HD 204827 dust cloud have quite small reddenings (E(B-V)$\sim$0.2 mag). In addition, they are low density diffuse ISM sightlines where the dust could have easily been subjected to processing by UV radiation and shocks (Gordon & Clayton 1998; Gordon et al. 2003). A group of similar sightlines

in the Galaxy sampling very low density ISM, showed weak bumps and steep non-CCM far-UV extinction (Clayton et al. 2000). But the weakness of the bumps and the steepness of the far-UV extinction of these sightlines do not approach that seen in the SMC. These Galactic sightlines are more similar to the those associated with LMC2 superbubble (Misselt et al. 1999; Gordon et al. 2003).

So the conditions for producing SMC-type extinction exist in our own galaxy. Those conditions are not necessarily associated with low reddening, low density, diffuse ISM environments. Also, metallicity differences between the Galaxy and the SMC may not be a determining factor. This supports results that find SMC-type extinction in starburst galaxies having a wide range of metallicities (Calzetti, Kinney, & Storchi-Bergmann 1994; Gordon et al.1997).

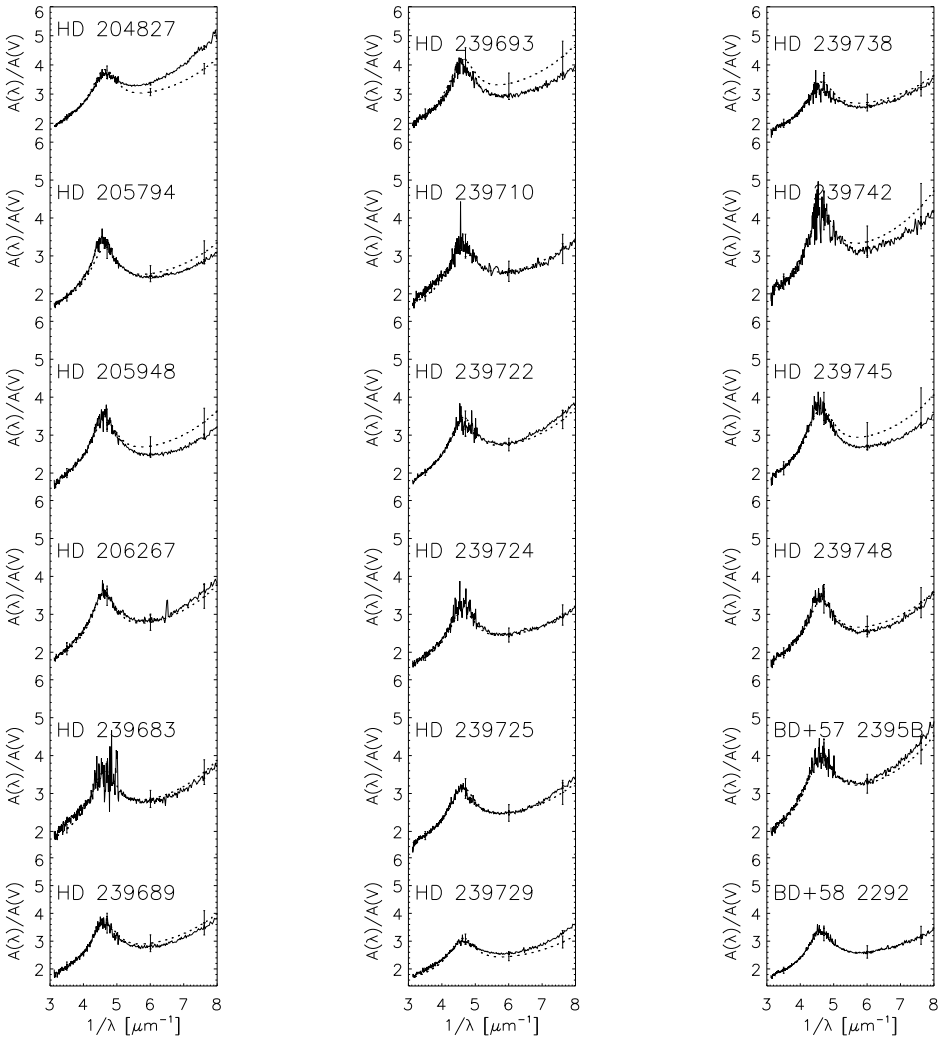

Figure 4.1: The extinction curves of the Trumpler 37 sightlines overlayed with CCM curves appropriate to R_V along each sightline. The error bars indicate a 1σ uncertainty.

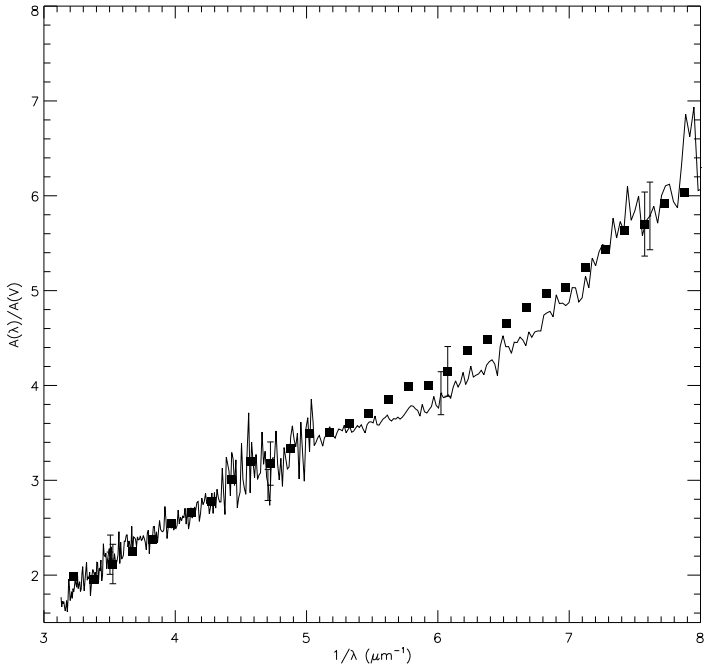

Figure 4.2: The partially dereddened extinction curve for HD 204827 (solid line). The extinction curve to the the SMC bar (squares) is from Gordon et al. (2003) is also shown. The error bars indicate a 1 σ uncertainty.

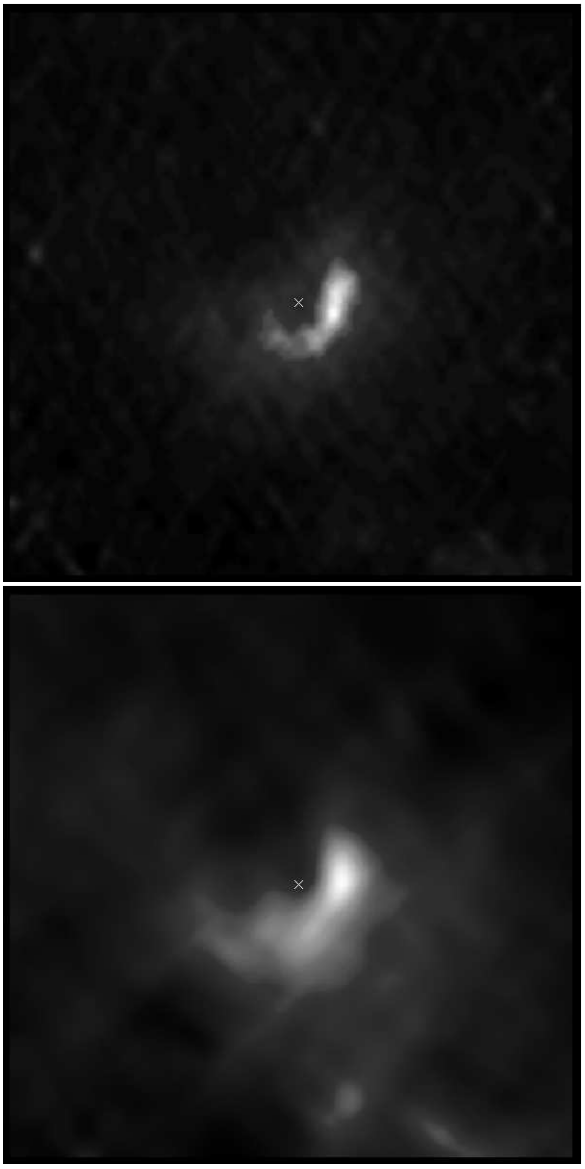

Figure 4.3: $0.5\,^{\circ} \times 0.5^{\circ}$ IRAS HiRes images of HD 204827 at 25 (top) and 60 μm (bottom), respectively. The x indicates the star's location.

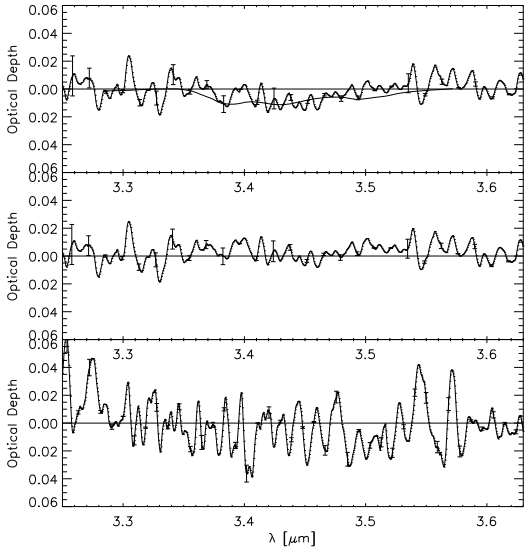

Figure 4.4: Optical depth plots of HD 204827 and HD 239722 for comparison. Both were obtained with SpeX. Top: HD 204827 with the C-H aliphatic stretch at 3.4 μm overlayed (de Vries et al. 1993). Middle: HD 204827 with the 3.4 μm feature removed for emphasis. Bottom: HD 239722; no feature is visible. The error bars represent 1 σ uncertainty.

5. Conclusions

This study constructed the largest homogeneous database of UV extinction curves, all of which have been fit by the FM relation and for which values of R_V have been calculated. All extinction curves and FM parameters have been normalized to A(V), rather than E(B-V), so that relationships between parameters may be more easily seen. It includes over 150 sightlines with d $>$ 2 kpc so the regions of the Galaxy beyond the solar neighborhood are well represented.

The main results of this study are:

(1.) The CCM extinction relation accurately describes the Galactic ISM in virtually all cases. This indicates that the physical processes which give rise to grain populations that have CCM-like extinction dominate the ISM, and thus, the quantity R_V can accurately describe the UV extinction for most sightlines. This implies that the grain populations responsible for different components of the extinction curve are being processed efficiently and systematically along most sightlines. Nevertheless, no one extinction curve, i.e. R_V=3.1, can accurately describe the average extinction properties of dust in a galaxy.

(2.) The bump width has a strong environmental dependence, with narrow bumps favoring diffuse sightlines, and broad bumps favoring dense sightlines. Also, very broad bumps are rare, as only 21 out of 426 sightlines had $\gamma > 1.1$. This suggests that the bump width may be related to mantling of

grains in dense environments, possibly by PAHs or ices, which are sensitive to disruption by UV radiation.

(3.) The central wavelength of the bump is invariant and may be regarded as a constant, with x_0=4.59±0.01. Unlike the other parts of the UV extinction curve, this parameter does not respond to different environments. The invariance of x_0, along with the observed variations in γ, put strong constraints on possible bump grain and mantle materials.

(4.) SMC- and LMC-like dust has been found in the Milky Way in regions which may have seen heavy grain processing. In the Magellanic Clouds, the conditions which give rise to such extinction are associated with low reddening, low density ISM; in the Galaxy, this may not necessarily be the case.

(5.) While there is evidence for shock processing in three of the four non-CCM sightlines, the common denominator is that all four sightlines have dense, molecule-rich clouds. Together, the sightlines in the Galaxy and the Magellanic Clouds suggest that similar extinction properties may arise from very different environments.

These results can be used to make more realistic grain models, thus making the corrections for extinction more accurate and providing insight into the nature of the grains themselves.

Bibliography

Abraham, P., Balazs, L. G., & Kun, M. 2000, A&A, 354, 645

Aiello, S., Guidi, I., Barsella, B., Penco, U., & Perinotto, M. 1982, Ap&SS, 87, 463

Aiello, S., Barsella, B., Chlewicki, G.,Greenberg, J. M., Patriarchi, P., & Perinotto, M. 1988, A&AS, 73, 195

Allain, T, Leach, S., & Sedlmayr, E. 1996, A& A, 305, 602

Allain, T, Leach, S., & Sedlmayr, E. 1996, A&A, 305, 616

Arenou, F., Lindegren, L., Froeschle, M., Gomez, A. E., Turon, C., Perryman, M. A. C., & Wielen, R. 1995, A&A, 304, 52

Aumann, H. H., Fowler, J. W., & Melnyk, M. 1990, AJ, 99, 1674

Barbaro, G., Mazzei, P., Morbidelli, L., Patriarchi, P., & Perinotto, M. 2001, A&A, 365, 157

Becker, W. & Fenkart, R. 1971, A&AS, 4, 241

Beegle, L. W., Wdowiak, T. J., Robinson, M. S., Cronin, J. R., McGehee, M. D., Clemett, S. J., & Gillette, S. 1997, ApJ, 487, 976

Bianchi, L., Clayton, G. C., Bohlin, R. C., Hutchings, J. B., & Massey, P. 1996, ApJ, 471, 203

Blaauw, A. 1996, BAN, 15, 265

Bless, R. C. & Savage, B. D. 1970, in Ultraviolet Stellar Spectra and Related Ground-Based Observations, IAU Symp. No. 36, eds. L. Houziaux and H.E. Butler, (Dordecht:Ridel), p. 28

Bohlin, R. C. Savage, B. D., & Drake, J. F. 1978, ApJ, 224, 132

Bohren C. F. & Huffman, D. R. 1983, Absorption and Scattering of Light by Small Particles (New York: Wiley Interscience)

Borgman, J., van Duinen, R. J., & Koornneef, J. 1975, A&A, 40, 461

Brown, A. G. A., Arenou, F., van Leeuwen, F., Lindegren, L., & Luri, X. 1997, in Hipparcos Venice 1997, eds. B. Battrick & M. A. C. Perryman (Paris: ESA), 63

Byram, E. T., Chubb, T. A., Friedman, H., & Kupperian, J. E., Jr. 1957, AJ, 62, 9

Calzetti, D., Kinney, A. L., & Storchi-Bergmann, T. 1994, ApJ, 429, 582

Cardelli, J. & Clayton, G. 1991, AJ, 101, 1021

Cardelli, J. A., Clayton, G. C., Mathis, J. S. 1988, ApJ, 329, 33

Cardelli, J., Clayton, G., & Mathis, J. 1989, ApJ, 345, 245

Cardelli, J. & Savage, B. 1988, ApJ, 325, 864

Cardelli, J., Sembach, K. R., & Mathis, J. S. 1992, AJ, 104, 1916

Cardelli, J. & Wallerstein, G. 1989, AJ, 97, 1099

Carnochan, D. J. 1986, MNRAS, 219, 903

Clayton, G. C. & Martin, P. G. 1985, ApJ, 288, 558

Clayton, G. C. & Fitzpatrick, E. L. 1987, AJ, 93, 157

Clayton, G. C., Anderson, C. M., Magalhaes, A. M., Code, A. D., Nordsieck, K. H., Meade, M. R., Wolff, Michael J., Babler, B., Bjorkman, K. S., Schulte-Ladbeck, R. E., Taylor, M., & Whitney, B. A. 1992, ApJ, 385, L53

Clayton, G. C., Gordon, K. D., & Wolff, M. J. 2000, ApJ, 129, 147

Clayton, G. C., Green, J., Wolff, M., Zellner, N., Code, A., Davidsen, A., WUPPE Science Team, & HUT Science Team, 1996, ApJ, 460, 313

Clayton, G. C., Gordon, K. D., Salama, F., Allamandola, L. J., Martin, Peter G., Snow, T. P., Whittet, D. C. B., Witt, A. N., & Wolff, Michael J. 2003, ApJ, 592, 947

Clayton, G. C., Wolff, M. J., Sofia, U. J. Gordon, K. D., Misselt K. A. 2003, ApJ, 588, 871

Cox, A. N. 2000, Allen's Astrophysical Quantities ed. A. N. Cox, (4th ed.; London: AIP Ltd.)

Crawford, I. A. 1992, Obs., 112, 161

Crutcher, R. M. 1985, ApJ, 288, 604

Cushing, M., Vacca, W., & Rayner, J. 2003, PASP, submitted

Cutri, R.M., et al. 2003, 2MASS Second Incremental All Sky Point Source Catalog

Daflon, S., Cunha, K., & Becker, S. R. 1999, ApJ, 522, 950

Danks, A. C., Federman, S. R., & Lambert, D. L. 1984, A&A, 130, 62

Désert, F.-X., Jenniskens, P., & Dennefeld, M. 1995, A&A, 303, 223

De Vries, M. S., Reihs, K., Wendt, H. R., Golden, W., Hunziker, H., Flemming, R., Peterson, E., & Chang, S. 1993, Geochim. Cosmochim. Acta, 57, 933

De Zeeuw, P. T., Hoogerwerf, R., de Bruijne, J. H. J., Brown, A. G. A., & Blaauw, A. 1999, AJ, 117, 354

Draine, B. T. & Lee, H. M. 1984, ApJ, 285, 89

Draine, B. T. 1985, ApJS, 57, 587

Draine, B. T. 1987, ApJS, 64, 505

Draine, B. T. 1989, IAUS, 135, 313

Draine, B. T. & Malhotra, S. 1993, ApJ, 414, 632

Duley, W. W. & Seahra, S. 1998, ApJ, 507, 874

Duley, W. W. & Seahra, S. 1999, ApJ, 522, L129

Eiroa C. & Hodapp, K.-W. 1989, A&A, 210, 345

Federman, S. R., Danks, A. C., & Lambert, D. L. 1984, ApJ, 287, 219

Federman, S. R. 1986, ApJ, 309, 306

Federman, S. R. & Lambert D. L. 1988, ApJ, 328, 777

Federman, S. R., Strom, C. J., Lambert, D. L., Cardelli, Jason A., Smith, V. V., & Joseph, C. L. 1994, ApJ, 424, 772

FitzGerald, M. P. 1970, A&A, 4, 23

Fitzpatrick, E. L. 1985, ApJS, 59, 77

Fitzpatrick, E. L. 1986, AJ, 92, 1068

Fitzpatrick, E. L. 1999, PASP, 111, 63 Fitzpatrick 2002

Fitzpatrick, E. & Massa, D. 1986, ApJ, 307, 286

Fitzpatrick, E. & Massa, D. 1988, ApJ, 328, 734

Fitzpatrick, E. & Massa, D. 1990, ApJS, 72, 163

Garrison, R. F. & Kormendy, J. 1976, PASP, 88, 865

Georgelin, Y. M. & Georgelin, Y. P. 1976, A&A, 49, 57

Gies, D. R. 1987, ApJS, 64, 545

Goebel, J. H. 1983, ApJ, 268, 41

Gordon, K., Calzetti, D., & Witt, A. 1997, ApJ, 487, 625

Gordon, K. & Clayton, G. 1998, ApJ, 500, 816

Gordon, K. D., Clayton, G. C., Misselt, K. A., Landolt, A. U., & Wolff M. J. 2003, preprint(astro-ph)/0305257)

Gredel, R., Pineau des Forets, G., & Federman, S. R. 2002, A&A, 389, 933

Hecht, J. 1981, ApJ, 246, 794

Hecht, J. 1986, ApJ, 305, 817

Henrard, L., Lucas, A. A., Lambin, P. 1993, ApJ, 406, 92

Henrard, L., Lambin, P., Lucas, A. A. 1997, ApJ, 487, 719

Hiltner, W. A. 1956, ApJS, 2, 389

Hiltner, W. A. & Johnson, H. L. 1956, ApJ, 124, 367

Hong, S. S. & Greenberg, J. M. 1980, A&A, 88, 194

Humphreys, R. M. 1978, ApJS, 38, 309

Jackson, J. D. 1962, in Classical Electrodynamics (New York: Wiley)

Jenniskens, P. 1994, A&A, 284, 227

Jenniskens, P., Ehrenfreund, P.; Désert, F.-X. 1992, A&A, 265, L1

Jenniskens, P. & Greenberg, J. M. 1993, A&A, 274, 439

Jones, A. P., Tielens, A. G. G. M., Hollenbach, D. J., & McKee, C. F. 1994, ApJ, 433, 797

Joseph, C. L., Snow, T. P. Jr., Seab, C., & Crutcher, R. M. 1986, ApJ, 309, 771

Kester, D. 1981, A&A, 99, 375

Koornneef, J. 1978, A&A, 68, 139

Koornneef, J. 1983, A&A, 128, 84

Koornneef, J. & Code, A. D. 1981, ApJ, 247, 860

Lada, E. A. & Blitz, L. 1988, ApJ, 326, L69

Larson, K. A., Whittet, D. C. B., & Hough, J. H. 1996, ApJ, 472, 755

Le Page, V., Snow, T., & Bierbaum, V. 2003, ApJ, 584, 316

Lee, W. & Wdowiak, T. J. 1993, ApJ, 410, L127

Léger, A., Verstraete, L., D'Hendecourt, L., Défourneau, D., Dutuit, O., Schmidt, W., & Lauer, J. 1989, IAUS, 135, 173

Li, A. & Greenberg, J. M. 1997, A&A, 323, 566

Luck, R. E. & Lambert, David L. 1992, ApJS, 79, 303

Marschall, L.A., & van Altena, W.F. 1987, AJ, 94, 71

Mason, B. D., Gies, D. R., Hartkopf, W. I., Bagnuolo, W. G. Jr., Brummelaar, T. T., & McAlister, H. A. 1998, AJ, 115, 821

Massa, D. & Savage, B. D. 1984, ApJ, 279,310

Massa, D. & Fitzpatrick, E. L. 1986, ApJS, 60 305

Massa, D., & Fitzpatrick, E. L. 2000, ApJS, 126, 517

Massa, D. Savage, B. D. & Fitzpatrick, E. L. 1983, ApJ, 266, 662

Mathis, J. S., Rumpl, W., & Nordsieck, K. H. 1977, ApJ, 217, 425

Mathis, J. 1990, ARA&A, 28, 37

Mathis, J. & Cardelli, J. 1992, AJj, 104, 1916

Mathis, J. S. 1994, ApJ, 422, 176

Mathis, J. S. & Whiffen, G. 1989, ApJ, 341, 808

Mermilliod, J.-C., Turon C., Robichon, N., Arenou, F., Lebreton Y. 1997, in Hipparcos Venice 1997, eds. B. Battrick & M. A. C. Perryman (Paris: ESA), 643

Meyer, D. M. & Savage, B. D. 1981, ApJ, 248, 545

Misselt, K. Clayton, G. & Gordon, K. 1999, ApJ, 515, 128

Morbidelli, L., Patriarchi, P., Perinotto, M., Barbaro, G., di Bartolomeo, A. 1997, A&A, 327, 125

Nandy, K., Thompson, G. I., Jamar, C., Monfils, A., & Wilson, R. 1975, A&A, 44, 195

Nandy, K., Thompson, G. I., Jamar, C., Monfils, A., & Wilson, R. 1976, A&A, 51, 63

Nandy, K., Morgan, D. H., Willis, A. J., Wilson, R., & Gondhalekar, P. M. 1981, MNRAS, 196, 955

Narayanan, V. K. & Gould, A., 1999, ApJ, 523, 328

Nichols, J.S. & Linsky, J.L. 1996, AJ, 111, 517

Nicolet, B. 1978, A&AS, 34, 1

O'Donnell, J. E. & Mathis, J. S. 1997, ApJ, 479, 806

Oka, T., Thorburn, J. A., McCall, B. J., Friedman, S. D., Hobbs, L. M., Sonnentrucker, P., Welty, D. E., & York, D. G. 2003, ApJ, 582, 339

Papaj, J., Krelowski, J., Wegner, W. 1991, MNRAS, 252, 403

Papaj, J. & Krelowski, J. 1992, AcA, 42, 211

Papoular, R., Conard, J., Guillois, O., Nenner, I., Reynaud, C., & Rouzaud, J.-N. 1996, A&A, 315, 222

Patel, N. A., Goldsmith, P. F., Heyer, M. H., Snell, R. L., & Pratap, P. 1998, ApJ, 507, 241

Pendleton, Y. J., Sandford, S. A., Allamandola, L. J., Tielens, A. G. G. M. & Sellgren, K. 1994, ApJ, 437, 683

Petrie, R. M. & Pearce, J. A. 1961, PDAO, 12, 1

Pinsonneault, M. H., Stauffer, J., Soderblom, D. R., King, J. R., Hanson, R. B. 1998, ApJ, 504, 170

Pitman, K. M., Clayton, G. C., & Gordon, K. D. 2000, PASP, 112, 537

Puget, J. L. & Léger, A. 1989, ARA&A, 27, 161

Rayner, J. T., Toomey, D. W., Onaka, P. M., Denault, A. J., Stahlberger, W. D., Vacca, M. C., Cushing, M. C., & Wang, S. 2003, PASP, 155, 362

Sandford, S. A., Allamandola, L. J., Tielens, A. G. G. M., Sellgren, K., Tapia, M., & Pendleton, Y. 1991, ApJ, 371, 607

Savage, B. D. 1975, ApJ, 199, 92

Savage, B. D.; Massa, D.; Meade, M.; Wesselius, P. R. 1985, ApJS, 59, 397

Schmidt-Kaler, T. 1982, Landolt-Bornstein: Numerical Data and Functional Relationships in Science and Technology, eds. K. Schaifers & H. H. Voigt (Springer-Verlag, Berlin), VI/2b

Seaton, M. J. 1979, MNRAS, 187, 73

Simonson, S. C. 1968, ApJ, 154, 923

Smith, R. G., Blum, R. D., Quinn, D. E., Sellgren, K., & Whittet, D. C. B. 2002, MNRAS, 330, 837

Smith, H. Jr. & Eichhorn, H. 1996, MNRAS, 281, 211

Smith, R. G., Sellgren, K., & Brooke, T. Y. 1993, MNRAS, 263, 749

Snow, T. P. Jr. & Seab, C. G. 1980, ApJ, 242, L83

Sofia, U. J., Cardelli, J. A., & Savage, B. D. 1994, ApJ, 430, 650

Sorrell, W. H. 1990, MNRAS, 243, 570

Spitzer, L. 1978, Physical Processes in the Interstellar Medium, (New York: John Wiley & Sons, Inc.)

Stecher, T. P. & Milligan, J. E. 1962, ApJ, 136, 1

Stecher, T. P. 1965, ApJ, 142, 1683

Steel, T. M. & Duley, W. W. 1987, ApJ, 315, 337

Thé, P. S.; Bakker, R.; Tjin A Djie, H. R. E. 1980, A&A, 89, 209

Tielens, A. 1989, IAUS, 135, 239

Thorburn, J. A., Hobbs, L. M., McCall, B. J., Oka, T., Welty, D. E., Friedman, S. D., Snow, T. P., Sonnentrucker, P., York, D. G. 2003, ApJ, 584, 339

Ugarte, D. 1995, ApJ, 443, L85

Vacca, W. D., Garmany, C. D., Shull, J. M. 1996, ApJ, 460, 914

Vallée, J. P. 2002, ApJ, 566, 261

Van Buren, D. & McCray, R. 1988, ApJ, 329, L9

Verstraete, L., Leger, A., D'Hendecourt, L., Defourneau, D., Dutuit, O. 1990, A&A, 237, 436

Ward-Thompson, D. & Robson, E. I. 1991, MNRAS, 248, 670

Warren, S. G. 1984, Appl. Optics, 23, 1206

Weingartner, J. C. & Draine, B. T. 2001, ApJ, 548, 296

Whittet, D. C. B. 1992, Dust In the Galactic Environment, (New York: IOP Publishing Ltd.)

Whittet, D. C. B., Bode, M., Longmore, A., Admason, A., McFadzean, A., Aitken, D., & Roche, P. 1988, MNRAS, 233, 321

Whittet, D. C. B. & van Breda, I. G. 1980, MNRAS, 192, 467

Whittet, D. Shenoy, S. Clayton, G. Gordon, K. 2003, in Astrophyics of Dust, in press

Will, L. M. & Aannestad, P. A. 1999, ApJ, 526, 242

Wu, C.-C., Mo, J., & Crenshaw, D. M. 1983, IUE Ultraviolet Spectral Atlas, IUE/NASA Newsletter No. 22

York, D. G., Drake, J. F., Jenkins, E. B., Morton, D. C., Rogerson, J. B., & Spitzer, L. 1973, ApJ, 182, L1

Appendix A: IUE Spectra of UV Comparison Stars

Table A.1: UV Comparison Stars

HD	Sp Type	Short Wavelength Spectra	Long Wavelength Spectra
164794	O5V	SWP 14163, 14194	LWR 10768, 10787
47839	O7V	SWP 08146	LWR 07077
214680	O9V	SWP 01764	LWR 01655
38666	O9.5IV	SWP 14340	LWR 10954
188209	O9.5Ia	SWP 08196	LWR 07123
36512	B0V	SWP 08164	LWR 07097
63922	B0III	SWP 09511	LWR 08237
204172	B0Ib	SWP 19249	LWR 15285
167756	B0Ia	SWP 06584, 06585, SWP 06586	LWP 26185, LWR 05635, LWR 05635
55857	B0.5V	SWP 14339	LWR 10953
34816	B0.5IV	SWP 08166	LWR 07099, 07100
119159	B0.5III	SWP 19245	LWR 15281
64760	B0.5Ib	SWP 07719, 19056	LWR 06706, 15100
150898	B0.5Ia	SWP 10173	LWR 08837
31726	B1V	SWP 08165	LWR 07098
46328	B1III	SWP 19244	LWR 15280
40111	B1Ib	SWP 08151	LWR 07081
91316	B1Iab	SWP 19501, 19520	LWR 15529
150168	B1Ia	SWP 19246	LWR 15282
74273	B1.5V	SWP 14307	LWR 10938
62747	B1.5III	SWP 19295, 19297	LWR 15328
64802	B2V	SWP 14308	LWR 10939
3360	B2IV	SWP 04316	LWR 03812
51283	B2III	SWP 08167	LWR 07101
165024	B2Ib	SWP 10174	LWR 08838
61831	B2.5V	SWP 14309	LWR 10940
63465	B2.5III	SWP 19296	LWR 15329
32630	B3V	SWP 08197	LWR 07125, 07126

continued on next page

Table A.1: *continued*

HD	Sp Type	Short Wavelength Spectra	Long Wavelength Spectra
42560	B3IV	SWP 19365	LWR 15403
79447	B3III	SWP 14338	LWR 10952
65904	B4V	SWP 15557	LWR 12042
202654	B4IV	SWP 19363	LWR 15401
195986	B4III	SWP 19248, 19292	LWR 15284
34759	B5V	SWP 15537	LWR 09868
78316	B8III	SWP 14053, 15696	LWP 05145, LWR 10710
		SWP 15790, 15804	LWR 12109, 12161
		SWP 15804, 15820	LWR 12175

Appendix B: UV Spectral Types

Table B.1: UV Spectral Types

HD	This work	CF88	Aiello et al. 1988	PK92
2905	B1 Iab	...	B1 Ia	...
13268	B0 Ib	...	O8 IV	...
14250	B1.5 III	...	B0.5 IV	...
14434	O5 V	...	O5-6 III	...
14442	O5 V	...	O5.6 III	...
14947	O5 V	...	O5 I	...
15558	O5 V	...	O5 III	...
15570	O5 V	...	O4 I	...
15629	O5 V	...	O5 V	...
16691	O5 V	...	O5 I	...
18352	B2 IV	...	B1 III-IV	...
23060	B3 IV	...	B2.5 V	...
23180	B1.5 III	...	...	B1 III
24263	B4 V	...	...	B5 V
30614	O9.5 Ia	...	O9.5 Ia	...
36629	B2 V	...	B2 V	...
36879	O9.5 IV	...	O6-7 V	...
37061	B0 V	...	B1 V	...
37367	B1 V	...	B2 IV-V	...
37903	B1.5 V	...	B1.5 V	...
38087	B4 V	...	B5 V	...
38131	B0.5 III	...	...	...
40893	O7 V	...	B0 IV	...
41117	B2 Ib	...	B2 Ia	...
42087	B2 Ib	...	B2.5 Ib	...
46056	O9.5 IV	...	O8 V	...
46106	B0.5 V	...	B0 V	...
46149	O9 V	...	O8.5 V	...
46150	O5 V	...	O6 V	...
46202	O9.5 IV	...	O9 V	...
46223	O5 V	...	O4 V	...
47129	O5 V	...	O8 III	...

continued on next page

Table B.1: *continued*

HD	This work	CF88	Aiello et al. 1988	PK92
47240	B1 Ia	...	B1 Ib	...
48434	B0.5 Ia	...	B0.5 II-III	...
52721	B1 V	...	...	B1 V
53974	B0.5 IV	...	B0 III	B0 V
54306	B1 V	...	B1.5 V	...
61827	B1.5 III	...	B3 Ia	...
73882	O7 V	...	O8 V	...
93028	O9.5 IV	...	O9 III-IV	...
93129	O5 V	...	O3 I	...
93205	O5 V	...	O3 V	...
93222	O7 V	...	O7 III	...
93250	O5 V	...	O3 V	...
93403	O5 V	...	O5 III	...
93843	O7 V	...	O5 III	...
96715	O5 V	...	O4 III	...
114213	B1 Iab	...	B1 Ia	...
120521	O9.5 Ia	...	O8-9 Ib	...
122879	B0 Ib	...	B0 Ia	...
123008	O9.5 Ia	...	O9.5 I	...
147701	B3 V	...	B5 V	...
147889	B2 V	...	B2 V	...
147933	B1 V	...	B2 IV	B2 V
149757	B0 III	...	...	O9.5 V
152233	O5 V	...	O6 III	...
152236	B2 Ib	...	B1.5 Ia	...
152245	B0.5 IV	...	O9 IV	...
152246	B0.5 Ia	...	O8.5 IV	...
152247	B0 Ia	...	B0 III	...
152248	O9.5 Ia	...	O7 Ib	...
152249	O9.5 Ia	...	O9.5 I	...
154445	B1 V	...	B0.5 V	B1 V
162978	O9.5 IV	...	O8.5 III	...
164492	O7 V	...	O7 V	...
164816	O9 V	...	O9 IV-V	...
165052	O7 V	...	O7 V	...
168076	O5 V	...	O4 V	...

continued on next page

Table B.1: *continued*

HD	This work	CF88	Aiello et al. 1988	PK92
168112	O5 V	...	O5 III	...
170740	B1 V	...	...	B2 V
179406	B2.5 V	...	...	...
190603	B2 Ib	...	B1.5 Ia	...
192281	O5 V	...	O5 V	...
193682	O5 V	...	O5 V	...
197512	B1 V	...	B1.5 V	...
198478	B2 Ib	...	B3 Ia	...
198781	B0.5 III	...	...	B0.5 V
199216	B2 III	...	B2 II	...
199579	O7 V	...	O6.5 III	...
200775	B1.5 V	...	B5 V	...
203532	B3 IV	...	...	B3 V
204827	B0 V	O9.5 V	...	...
205794	B0.5 V	B0.5 V	...	...
205948	B1 V	B1 V	...	...
206267	O7 V	O6 V	...	...
207198	B0 Ib	...	O9 II-III	...
209339	O9.5 IV	...	O9 V	B0 V
215835	O5 V	...	O6 V	...
216898	O9 V	...	O9 V	...
217086	O5 V	...	O7 V	...
229196	O5 V	...	O6 III	...
236923	B1.5 V	...	B2.5 III	...
239683	B2 IV	B3 IV	...	...
239689	B1 V	B1.5 V	...	...
239693	B4 IV	B3 V	...	...
239710	B1 V	B2.5 V	...	...
239722	B1 V	B2 IV	...	...
239724	B1.5 III	B1 III	...	...
239725	B1 V	B2.5IV-V	...	...
239729	O9 V	B0 V	O9 V	...
239738	B2 V	B2 IV	...	...
239742	B4 IV	B2 V	...	...
239745	B1.5 V	B1 V	...	...
239748	B1 V	B1 V	...	...

continued on next page

Table B.1: *continued*

HD	This work	CF88	Aiello et al. 1988	PK92
242908	O5 V	...	O4 V	...
251204	B0 III	...	B0 III	...
252325	B0 V	...	B0-1 V	...
303308	O5 V	...	O3 V	...
326329	B0.5 Ib	...	B2.5 III	...
326330	B1.5 V	...	B0.5 V	...
BD+45 973	B0.5 V	...	B1 V	...
BD+55 393	B1 V	...	B2 V	...
BD+60 497	O7 V	...	O6 V	...
BD+60 594	O9 V	...	O8.5-9 V	...
BD+63 1964	B0 Ib	...	B0-0.5 I	...
BD+57 2395B	B2 V	B3 V	...	...
BD+58 2292	B2 V	B2 IV-V	...	...
CD-59 3300	O5 V	...	O6 V	...

Appendix C: Permission Letter

From marvel@aas.org Tue Sep 16 20:23:08 2003

Return-Path: <marvel@aas.org>

Received: from server.marvelhome (dsl092-150-249.wdc2.dsl.speakeasy.net [66.92.150.249]) by theory.phys.lsu.edu (8.11.6+Sun/8.11.6) with ESMTP id h8H1N7o12075 for <valencic@baton.phys.lsu.edu>; Tue, 16 Sep 2003 20:23:07 -0500 (CDT)

Received: from knotebook ([192.168.1.113]) by server.marvelhome (8.11.2/8.11.2) with ESMTP id h8H0Efp27440 for <valencic@baton.phys.lsu.edu>; Tue, 16 Sep 2003 20:14:42 -0400

Reply-To: <marvel@aas.org>

From: "Kevin Marvel" <marvel@aas.org>

To: "'Lynne Valencic'" <valencic@baton.phys.lsu.edu>

Subject: RE: permission to use MS #58355

Date: Tue, 16 Sep 2003 21:10:37 -0400

Organization: American Astronomical Society

Message-ID: <002401c37cb8$814fc060$7101a8c0@aas.org>

MIME-Version: 1.0

Content-Type: text/plain; charset="us-ascii"

Content-Transfer-Encoding: 7bit

X-Priority: 3 (Normal)

X-MSMail-Priority: Normal

X-Mailer: Microsoft Outlook, Build 10.0.3416

In-Reply-To: <20030916140036.B4689@theory.phys.lsu.edu>

X-MimeOLE: Produced By Microsoft MimeOLE V6.00.2800.1165

Importance: Normal

Status: RO

Content-Length: 1291

Lines: 45

Lynne,

By contacting us with your decision to reprint your first author paper in your dissertation in its entirety, you have fulfilled all necessary obligations to go forward with the reproduction.

Kev.

Original Message:

From: Lynne Valencic [mailto:valencic@baton.phys.lsu.edu]

Sent: Tuesday, September 16, 2003 3:01 PM

To: copyright@aas.org

Subject: permission to use MS #58355

Dear Sir or Madam,

I am the first author on the paper entitled "Small Magellanic Cloud- Type Interstellar Dust in the Milky Way", MS #58355, accepted for publication in the Nov 20, 2003 ApJ (Valencic et al. 2003, ApJ, 598, 1). I would like permission to reproduce this paper in its entirity as a chapter in my disserta-

tion. Please respond to this email to confirm or deny permission. Both this email and your response will be shown in the dissertation's Appendix.

Thank you,

Lynne A. Valencic

Vita

Lynne Angela Valencic was raised in Cleveland, Ohio. She received her bachelor of science degree from Case Western Reserve University in 1993 and attended graduate school at Louisiana State University in Baton Rouge. She expects to receive her Doctor of Philosophy degree in December of 2003.